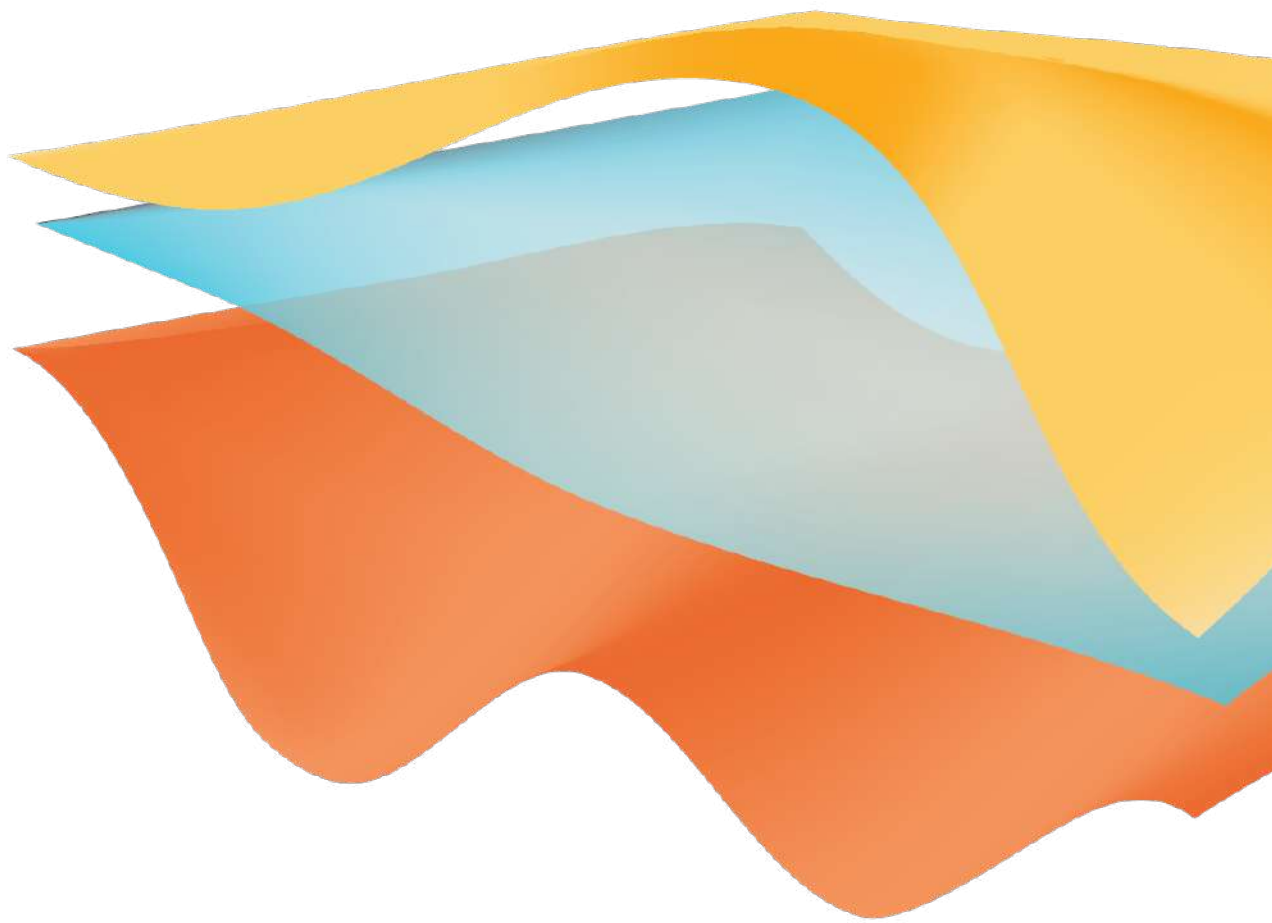


Analyzing out-of-plane deformations caused by varying Poisson ratio distributions in a metamaterial

Master Thesis by [Anna van Soest](#)



Department of Precision and Microsystems Engineering

Analyzing out-of-plane deformations caused by varying Poisson ratio distributions in a metamaterial

A.M.J. van Soest | 4440404

Report no : 2023.xxx
Professor : Prof. dr. ir. J.L. Herder
Daily supervisor : Dr. ir. F. G. J. Broeren
Daily supervisor : Dr. ir. W. W. P. J. van der Sande
External member : Dr. ir. M. J. Mirzaali
Specialisation : BioMechanical Design
Type of report : Master Thesis
Date : August 10, 2023

Analyzing out-of-plane deformations caused by varying Poisson ratio distributions in a metamaterial

by

A.M.J. van Soest

to obtain the degree of Master of Science
at the Delft University of Technology.

Student number:	4440404	
Project duration:	April, 2022 – August, 2023	
Thesis committee:	Prof. dr. ir. J. L. Herder,	TU Delft, chair
	Ir. E. G. J. Broeren,	TU Delft, daily supervisor
	Ir. W. W. P. J. van der Sande,	TU Delft, daily supervisor
	Ir. M. J. Mirzaali,	TU Delft, external member

An electronic version of this thesis is available at <http://repository.tudelft.nl/>.

Preface

When I started my masters degree, we were in the middle of the Covid pandemic. Just as everyone else, I worked from home and to stay motivated I sometimes studied together with a friend at my kitchen table. It only seems fitting now, a Tuesday night at 20.34 pm, that I write one of the final pieces of my master thesis at my kitchen table. One of the first courses I took was a course on compliant mechanisms. The possibilities of compliant mechanisms intrigued me and when the time came to find a thesis subject, I went to look within the compliant mechanism group. Here I found the exciting area of metamaterials and more notably the auxetic metamaterials. Due to the auxetic capability, the meta-material deforms into a dome under out-of-plane deformation. The deformation ability of an auxetic metamaterial became the subject of my master thesis.

I could not have completed this research without my daily supervisors Freek Broeren and Werner van de Sande. I want to thank them for the guidance and support they have provided throughout the last year. Every week we would meet and have insightful discussions during which we explored and understood the topic more. Next, I would also like to thank Just Herder for interesting discussions and providing his expertise when necessary. Moreover, I would like to thank everyone from the ShellSkeleton group for always offering their help and bringing lively discussions. I also want to thank Tirza Izelaar for making the beautiful cover of this master thesis. Ofcourse, I can't forget my friends for being there for the laughs and distraction. More notably, I want to thank my parents for their continuous support. Last but not least, I would like to thank Dirk-Jan Boonstra for supporting me throughout the whole project and cheering me on whenever necessary.

A.M.J. van Soest
Delft, August 2023

Contents

1	Introduction	1
2	The functionalities exhibited by elastic and planar mechanical metamaterials	3
1	Introduction	3
2	Constraints and categorization	4
2.1	Constraints	4
2.2	Categorization	4
3	Theory background	5
3.1	Chirality	5
3.2	Hierarchy	6
3.3	Negative stiffness behavior	6
4	Results	6
4.1	Oblique lattice	7
4.2	Rectangular lattice	7
4.3	Square lattice	10
4.4	Hexagonal lattice	13
5	Discussion	15
5.1	Oblique lattice	15
5.2	Auxetic	16
5.3	Zero Poisson's ratio	17
5.4	Stress distribution	17
5.5	Multi-stability	17
5.6	Shape reconfiguration	18
5.7	Shape fitting	18
6	Conclusion	18
3	Analyzing out-of-plane deformations caused by varying Poisson ratio distributions in a metamaterial	23
1	Introduction	23
2	Background	24
2.1	Auxetic and synclastic deformation	24
2.2	Pure bending	25
2.3	Numerical integration	25
3	Method	25
3.1	Simulation model	26
3.2	Pure bending	26
3.3	Numerical integration	26
3.4	COMSOL setup	26
3.5	Poisson's ratio	27
3.6	Error measurement	28
4	Results	29
4.1	Effect of a varying Poisson's ratio distribution	29
4.2	Comparison analytical model and COMSOL model	30
4.3	Shape following	30
5	Discussion	31
6	Conclusion	33
A	Poisson's ratio gradient and the corresponding displacement field	35
A.1	S-curve	35
A.2	Parabolic	36
A.3	Cosine 1D	37
A.4	Cosine 2D	37
B	Comsol data-processing	38
C	Matlab code	39
D	Comsol and Matlab overlap uniform Poisson's ratio	42

1

Introduction

Over the last decade, research has been conducted into obtaining unusual material properties. A material that exhibits a negative or zero property, for example negative compressibility or a negative Poisson's ratio, are named metamaterials. The desired mechanical property is achieved by carefully modifying the macro-structure of the material (1). Metamaterials have been mainly researched on their own accord and not in a combination with another engineering field. One of the possible engineering fields in which a metamaterial might be applied is that of shell mechanisms. A combination would be interesting because shell mechanisms and mechanical metamaterials have overlapping functionalities such as negative stiffness or shape fitting (2). The combination might enhance the shared functionality.

The literature study, chapter 2, investigates which functionalities are found in planar and elastic metamaterials. The planar and elastic requirement is set to ensure that the examined metamaterial can be used as a building block in a shell mechanism. To provide a clear overview, the reviewed metamaterials are categorized according to the geometrical shape of the unit cell. The reviewed functionalities are: auxetic, (near) zero Poisson's ratio, stress distribution, negative stiffness, shape fitting and shape reconfiguration.

From the literature study it became apparent that the auxetic functionality is researched most often. Most of the auxetic materials had a Poisson's ratio range from $\nu = -1$ to $\nu = 0$. A negative Poisson's ratio also alters the out-of-plane deformation of the material. However, this novel ability is often not further explored. One of them is quite interesting, namely the ability of an auxetic material to deform into a dome. With a positive Poisson's ratio, the out-of-plane deformation would be saddle-shaped. Dome-shaped deformation is named synclastic deformation and saddle-shaped anticlastic deformation. Synclastic deformation resulting from an auxetic material is analyzed from an application and experimental point of view (3; 4).

A combination of synclastic and anticlastic deformation in one plane is also possible with a metamaterial. Part of the metamaterial would be auxetic and the other part would have a positive Poisson's ratio. This combination is analyzed mainly from an experimental and computation point of view (5; 6). An analytical understanding seems to be missing for a synclastic deformation and for the combination of synclastic and anticlastic deformation.

A study, chapter 3, is set up that proposes an analytical model to understand the relation between the Poisson's ratio and the out-of-plane deformation based on a pure bending approach. To analyze every type of deformation, four Poisson's ratio gradient variants are applied in the analytical model. The output of the analytical model is compared against the output of the FEM software Comsol to determine the limitations of the proposed analytical model.

The study shows that various desired curved shapes can be achieved by varying the Poisson's ratio across the material, for example an egg shape or wave shape. The proposed analytical model has a Mean Absolute Percentage Error (MAPE) between 88.07% and 99.77%. The analytical model is a next step in determining the Poisson's ratio gradient required for a desired shape. Next steps would include enhancing the proposed model by analyzing other Poisson's ratio gradients. Another step would be to include more details in the model, such as symmetry and displacement in every direction.

A new range of shape forming possibilities is opened with the rise of metamaterials, specifically with auxetic materials. Hopefully the reader of this report will feel inspired to further develop interesting out-of-plane deformations by seeing the effect of a Poisson's ratio gradient.

Bibliography

[1] A. A. Zadpoor, "Mechanical meta-materials," *Materials Horizons*, vol. 3, no. 5, pp. 371–381, 2016.

-
- [2] K. A. Seffen, "Compliant shell mechanisms," *Philosophical Transactions of the Royal Society A: Mathematical, Physical and Engineering Sciences*, vol. 370, no. 1965, pp. 2010–2026, 2012.
- [3] M. Sanami, N. Ravirala, K. Alderson, and A. Alderson, "Auxetic materials for sports applications," *Procedia Engineering*, vol. 72, pp. 453–458, 2014.
- [4] M. J. Mirzaali, A. Ghorbani, K. Nakatani, M. Nouri-Goushki, N. Tümer, S. J. Callens, S. Janbaz, A. Accardo, J. Bico, M. Habibi, *et al.*, "Curvature induced by deflection in thick meta-plates," *Advanced materials*, vol. 33, no. 30, p. 2008082, 2021.
- [5] R. La Magna and J. Knippers, "Tailoring the bending behaviour of material patterns for the induction of double curvature," in *Humanizing Digital Reality: Design Modelling Symposium Paris 2017*, pp. 441–452, Springer, 2018.
- [6] Y. Sakai and M. Ohsaki, "Optimization method for shape design of auxetic bending-active gridshells using discrete differential geometry," in *Structures*, vol. 34, pp. 1589–1602, Elsevier, 2021.

2

The functionalities exhibited by elastic and planar mechanical metamaterials

Abstract

In the past years, mechanical metamaterials have been widely researched because of its many curious functionalities. However, experimental applications of a mechanical metamaterial into another mechanisms is yet to be researched as extensively. An interesting application would be a shell mechanisms because they often have been designed for similar functionalities as mechanical metamaterials. Such an application would constrain the mechanical metamaterial design to be planar and flexible. In order to properly choose the desired mechanical metamaterial, a literature overview is provided of various designs and their functionalities. The mechanical metamaterial designs are categorized in a geometrical manner according to the 2D Bravais lattices (oblique, rectangular, square and hexagonal). The found functionalities are auxetic behavior, (near) zero Poisson's ratio, stress distribution, negative stiffness behavior, bi-/multi-stability, shape reconfiguration and shape fitting. It is found that none of the reviewed mechanical metamaterial designs fit into the oblique Bravais lattice category. In the other three Bravais lattice categories, almost every functionality is exhibited except for shape reconfiguration and shape fitting which are found, respectively, within the reviewed hexagonal Bravais lattices, and the square and rectangular Bravais lattices. The literature review provides an overview of which functionalities are exhibited by which Bravais lattice to aid the reader in choosing the best design for the desired experimental application.

1. Introduction

Materials found in nature exhibit a definite range of mechanical properties. Their properties range from optical to acoustical and from chemical to mechanical. Collectively, they describe a materials behavior. However, the range is limited. An emerging field that seeks to extend the limits of material properties, is that of metamaterials. Metamaterials have an internal structure that is designed and tailored to create extraordinary properties (1). Meta-materials have shown to be able to alter acoustic properties (2), optical properties (3) and mechanical properties (4; 1). Mechanical metamaterials try to expand the mechanical range and additionally exhibit properties that do not occur naturally (4). Of the various metamaterials, the mechanical metamaterials are the youngest and thus less explored, though they bring an interesting range of properties (1). The properties are, for example, negative stiffness behavior (5; 6), or auxetic behavior (7).

Although mechanical metamaterials have been explored in recent years, application experiments are missing. Most review papers on mechanical metamaterials discuss their properties and sometimes speculate on possible engineering applications (1; 4). A potential and currently under-explored implementation is the use of mechanical metamaterials as a building block within a shell mechanism to extend or aid the shell's main properties. Structural shells are already commonly applied in architecture due to the good weight to load bearing ratio (8). More recently, the attention is starting to drawn towards using the elastic deformation of a shell, thus creating a shell mechanism. A shell mechanism is an object that is spatially curved and thin-walled (9). Due to its elastic deformation, the shell can transmit both force and motion (9). Shell mechanisms are widely researched and they have proven to become bi-stable and obtain zero stiffness (10; 11), which are to properties that are also often exhibited by mechanical metamaterials. Coupling two mechanisms with the same property might aid or extend the specific property. For example, a parallel combination of two springs with an opposite stiffness curve will provide a zero-stiffness motion (12). Shell mechanisms are very effective in their functionality and thus an implementation with the right mechanical metamaterial might become promising in practical applications.

However, depending on the desired functionality that one wants to enhance, various mechanical metamaterials might be correct. In order to be suitable for implementation in a shell mechanism, the mechanical metamaterial

must be planar and elastic. Of these mechanical metamaterials, the main functionality of each design is of interest. This creates the research question for this literature review: *Which functionalities are exhibited by planar and elastic mechanical metamaterials?*

The elaboration on the required properties can be found in section 2. Mechanical metamaterials can be categorized according to their primitive unit cell geometry. The method for this categorization is commented on in section 2. Next, in section 3, general background knowledge is provided. Afterwards, in section 4, the results are introduced. In this section, the functionalities are analyzed and ordered according to the set categorization. The found results will be further discussed in section 5. Finally, in section 6, this literature review is concluded.

2. Constraints and categorization

If one would conduct a review search on mechanical metamaterials, many papers would pop up. Many of which are not applicable to shell mechanisms. Constraints are needed to narrow down the search and select mechanical metamaterials that are applicable to shell mechanisms. This section elaborates on the constraints put on the analyzed papers. To make the many mechanical metamaterial designs organized and comprehensible, they are categorized according to the shape of their primitive unit cell.

2.1. Constraints

This review considers planar and elastic mechanical metamaterials. For an implementation in shell mechanisms, their four main components are reviewed to determine to which criteria the mechanical metamaterial should hold. First, a shell mechanism is small in one of the three dimensions. To accommodate the first criterium, planar metamaterials are more interesting than their three-dimensional (3D) counterparts. This is mainly because a 3D unit cell introduces additional complexity to the mechanism. Due to the mechanical metamaterial being small if used in its 3D form, a line of periodic unit cells might result in a corrugation instead of the desired mechanical properties. It is thus unsure if the desired mechanical effects will be shown. By using a planar mechanical metamaterial, the mechanical properties of the unit cell are still able to translate to the entire mechanical behavior of the shell mechanism.

Secondly, a shell mechanism is curved within its main plain so a planar mechanical metamaterial is a bit contradicting. However, if an area within the shell mechanism, or maybe the whole shell mechanism, can be differentiated, that area can then be considered a differentiable manifold. A property of a differentiable manifold is that it locally can be viewed as planar. Consequently, a planar mechanical metamaterial unit cell can be applied in that area.

Thirdly, the shell mechanism is infinitely stiff in its main plain. Again, this does not correspond to the flexibility of a mechanical metamaterials. This can be seen as an obstruction, or as an expansion on the capabilities of shell mechanisms.

Finally, because the shell mechanism has a behavior that is reversible, the analyzed mechanical metamaterial has a elastic deformation to allow the shell mechanism to return to its original state.

This leads to the mechanical metamaterials that will be analyzed in this review to be planar and elastic.

2.2. Categorization

This literature review categorizes the suitable mechanical metamaterial that fit to the mentioned criteria according to the categorization of the two-dimensional (2D) Bravais lattices. Bravais lattices are a categorization from crystallography and describe in the structuring of crystal grids, with recently the addition to describe mechanical structures (14). The four Bravais lattices describe every periodic mechanical metamaterial that is reviewed in this literature review. The 2D Bravais lattices are listed below and seen in Figure 2.2. Every lattice is described by its lattice vector

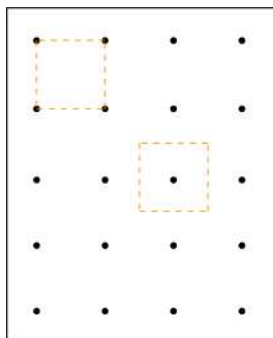


Figure 2.1: A lattice point (black dots) grid with square primitive unit cells indicated with orange dotted lines. One primitive unit cell has a lattice point at each corner and the other has a lattice point in the center.

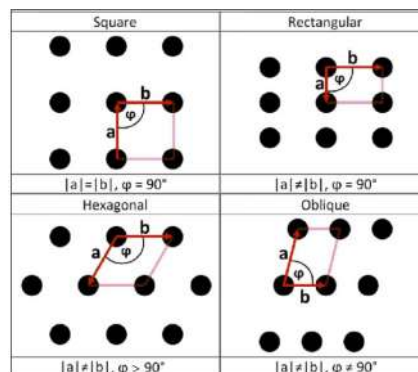


Figure 2.2: The four 2D Bravais lattice categories (13).

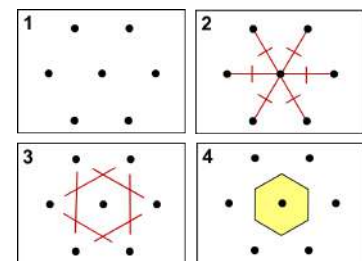


Figure 2.3: A step-by-step explanation of the construction of the Wigner-Seitz cell. The lattice points are defined (1) and lines are drawn from one lattice point to all neighbouring lattice points (2). An orthogonal line is placed on the previous construction lines (3). The orthogonal lines are kept (4) and their intersection creates the Wigner-Seitz cell (4).

parameters \mathbf{a} and \mathbf{b} and by the angle between the lattice vectors ϕ :

- Oblique
- Rectangular
- Square
- Hexagonal

To determine in which Bravais lattice category the mechanical metamaterial design falls, the shape of the primitive cell is observed. The primitive unit cell is the smallest possible unit cell of a structure and only contains one lattice point. This lattice point is assembled from the quarters of the lattice point that are at the corners of the primitive cell or there is one lattice point at the center of the primitive cell (15), as clarified in Figure 2.1. The primitive cell can in turn build up the whole system by pure translation and is space-filling (16; 1). By using a primitive cell, the mechanical metamaterial can be placed over a large area. A useful property of this cell is when it is made into a grid, the mechanical properties are guaranteed over any grid size. To correctly determine the primitive cell, the Wigner-Seitz constructed method is used. The resulting primitive unit cell is then ordered to their corresponding Bravais lattice. The construction of the Wigner-Seitz cell is done according to (Kettle, 1994)(17). A grid of lattice points is defined and from one lattice point, lines are drawn to the neighboring lattice points. At the center of the drawn lines, an orthogonal line is constructed. The intersection of the orthogonal lines define the Wigner-Seitz cell. A step-by-step view is seen in Figure 2.3.

Within each Bravais lattice section, the main functionalities are elaborated upon which were found during the analysis. The included functionalities are:

- Auxetic
- (near) Zero Poisson's ratio
- Stress distribution
- Bi-/multi-stability
- Shape fitting
- Shape reconfiguration

Not all functionalities are included in each geometrical section, as it was not explicitly mentioned in the reviewed papers.

For further understanding in this literature review, lattice vectors will refer to the enclosing sides of the primitive unit cell. Ligaments refer to the physical beams in the unit cell.

3. Theory background

Several terms are mentioned more than once throughout this literature review. To avoid repetition and for clarification they are defined in this separate chapter. The terms that are discussed here are chirality, hierarchy and negative stiffness behavior.

3.1. Chirality

The phenomenon of chirality stems from the world of chemistry and is mainly used to describe the structure of atoms. The definition of chirality is:

The property of an object that it can not be superimposed on its mirror image (18).

The most common example is that of a human hand. Human hands are each others mirror image, but one hand is not superimposable on the other. Regardless the orientation of the hand, neither translation nor rotation will cause them to coincide across all axes.

Within mechanical metamaterials, chiral structures are most often made of a central circular node that is tangentially connected to another circular node (4; 19). An example of this can be seen in Figure 2.6. The number of ligaments attached determines how the chiral material is called, i.e. a tetra-chiral material has four connecting ligaments and a hexa-chiral has six connecting ligaments (19). A material can also be called anti-chiral, where the ligaments connect to an adjacent node from the same side. Anti-chiral materials only exist for unit cells which have an even number of ligaments (19; 20).

3.2. Hierarchy

Any structure contains one or multiple elements that build up the structure. Such a structure becomes hierarchical once an element has an internal structure. This can be seen in Figure 2.4a, in which we see a structural honeycomb element. The beams of the honeycomb have an internal re-entrant honeycomb structure, thus creating a hierarchical material. A hierarchical element is defined by the order of hierarchy which defines the levels of scale (21). A good example of a hierarchical structure is the Eiffel tower. At its base, the Eiffel tower can be described as a curved triangle shape in which hierarchy is added by implementing an internal structure in the curved beams. Hierarchies can be introduced to mechanical metamaterials when a higher material strength is desired, while minimizing the overall weight. Another reason could be to increase the stretchability of the material (22; 21). Two examples of hierarchical metamaterials are seen in Figure 2.4.

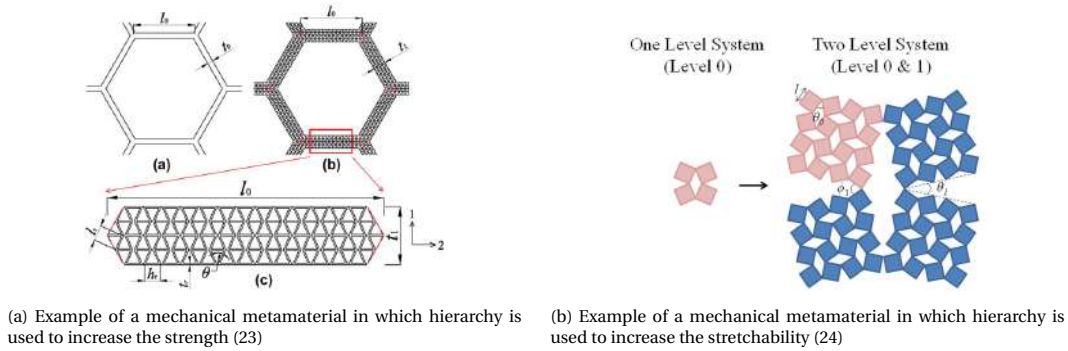


Figure 2.4: Two examples of units cells which use specific hierarchies to adjust material properties

3.3. Negative stiffness behavior

Negative stiffness behavior is usually seen in materials that contain elastic instabilities. The mechanism exhibits a buckling behavior and shifts from one stable state to another. Beyond a critical force level, the material will buckle and will cause a stage at which the material will switch to a different stable position on its own. This is featured by a negative slope in the stress-strain or force-displacement curve (25), as seen in Figure 2.5 which shows a force-displacement curve of an arched beam. Well-known examples are the lid of a lip balm can which needs to buckle in order to open, or a jumping popper toy which snaps to a stable state during the jump.

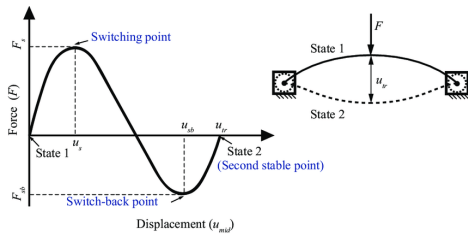


Figure 2.5: A force-displacement curve of an arched beam. The arched beam is visualised on the right and has a deformation from state 1 to state 2 over a displacement u_{tr} . The force required to obtain this displacement shows a negative slope in the graph on the left which indicated a negative stiffness behavior (26)

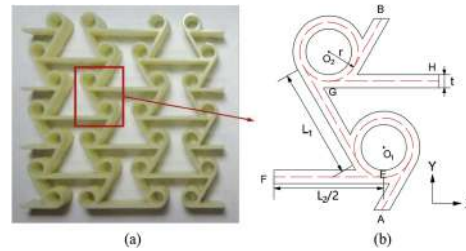


Figure 2.6: Example of a tri-chiral mechanical metamaterial. Three ligaments are connected from one circular node to another circular node (27)

4. Results

The results chapter is sectioned according to the four Bravais lattice types: oblique, rectangular, square and hexagonal. Each section elaborates on the functionalities found within the corresponding Bravais lattice category. Additionally, it is of importance to know which functionality come from which mechanical metamaterial structure. Thus, it is laid out which metamaterial structure corresponds to a specific functionality. Finally, it is analyzed if the functionality behavior changes when a parameter dimension is changed.

A total of 45 papers were reviewed for this literature. Some were double categorized because they contain configurations for two or more Bravais lattice categories. The breakdown of the number of papers reviewed per property and per geometrical category is seen in Figure 2.7a. Note that the figure with the breakdown of the auxetic property is in Figure 2.7b because otherwise it would have limited the readability of the first figure. For the oblique, rectangular, square and hexagonal lattices, respectively 0, 20, 17 and 21 papers are included in this literature study.



(a) An overview of the number of papers that is arranged according to the functionality and the geometrical category

(b) An overview of the number of papers reviewed that contain auxetic behaviour and arranged according to the geometrical category

Figure 2.7: Two overviews that indicate the number of papers found per category and per functionality. The auxetic overview is visualised separately to improve the readability of the other overview. The rectangular, square and hexagonal categories are visualised in orange, yellow and green respectively

4.1. Oblique lattice

The first Bravais lattice is the oblique lattice. Its main characteristic is that the two lattice vectors do not have the same dimension. The lattice vector dimension are noted with a and b . For an oblique lattice the relation between the lattice vectors is thus $a \neq b$. The angle between the lattice vectors may vary but it must be smaller than a perpendicular angle, thus $\phi \neq 90^\circ$ (28). The oblique lattice is visualized in the bottom right in Figure 2.2.

Interestingly, there were no papers reviewed that fit into this geometric category. Some materials may have an oblique angle within its unit cell structure. However, the unit cell itself is not oblique. Examples of this can be found in subsection 4.2.

4.2. Rectangular lattice

The Bravais lattice that will be discussed secondly is the rectangular lattice. Similar to the oblique lattice, the two connecting lattice vectors do not have the same dimension, thus $a \neq b$. Compared to the oblique lattice, the rectangular lattice has a perpendicular angle $\phi = 90^\circ$ (28). The general example of the rectangular lattice can be found in the top right corner of Figure 2.2 in Section 2. The lattice point grid configuration that results in a rectangular primitive unit cell is visualised in Figure 2.8. A few structural designs of rectangular lattices are provided in Figure 2.9.

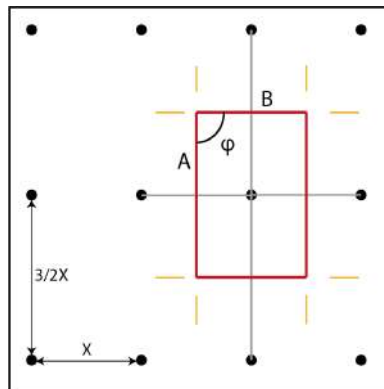


Figure 2.8: The lattice point grid configuration which results in a rectangular primitive unit cell. The construction of the Bravais lattice is done according to the Wigner-Seitz cell method. The block dots represent the lattice points. One central lattice point is chosen and is connected to the neighbouring lattice point which is visualised with grey lines. An orthogonal yellow line is placed at the center of the grey line. The intersection of the yellow lines then provide the Bravais lattice in red lines. If the horizontal and vertical distance are not equal, the primitive cell will be rectangular

A few rectangular lattices can be recognized by a repeating zig-zag pattern. An example of this can be seen in kirigami patterns, such as in Figure 2.9b, with straight ligaments that are connected in a zig-zag pattern (33) or in a Miura-ori sheet (34; 35). While these may seem as an oblique lattice at first sight, when a Wigner-Seitz cell is constructed it is clear that the primitive cell is rectangular, see Figure 2.10. Five functionalities were found within the rectangular Bravais lattice designs. The functionalities found are auxetic (33; 29; 32; 35; 34; 36; 30), zero Poisson's ratio (32; 37), stress distribution (31; 32; 37; 38; 36), multi-stability (37; 39; 38; 35) and shape fitting (36; 35).

Auxetic

Within the rectangular mechanical metamaterials, three different structures are found that exhibit auxetic behavior. The first one is based on the zig-zag pattern. Whether a material with a zig-zag pattern is auxetic depends on which

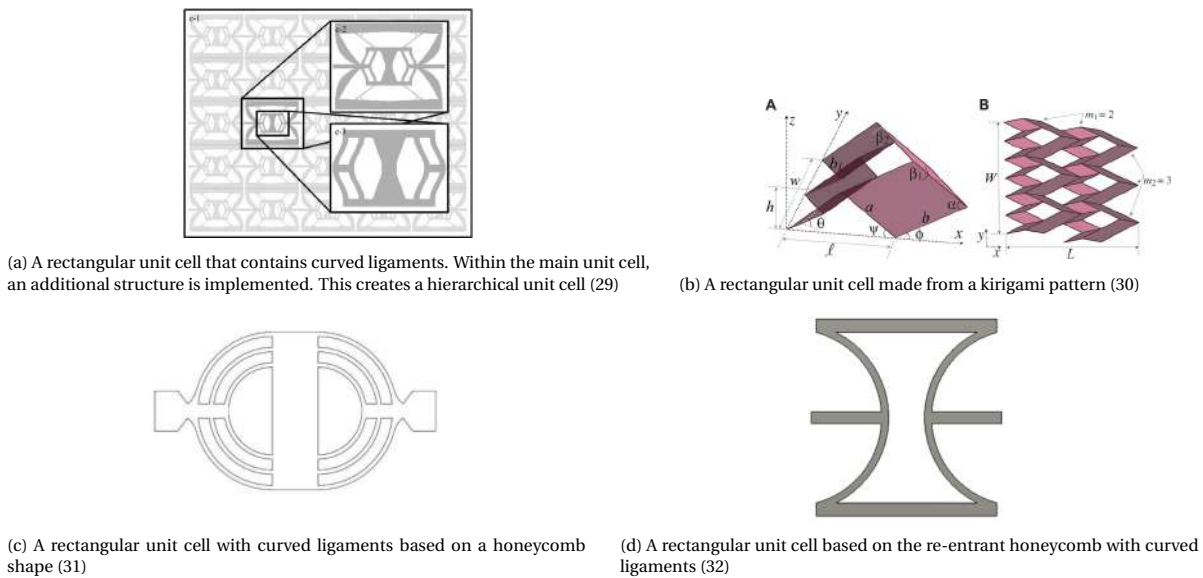


Figure 2.9: Four examples of rectangular unit cells with varying internal structures

deformation mode is dominant. Under compression of the material, a zig-zag pattern may have two different deformation modes. The ligaments will either stack or they will buckle depending on the stiffness and/or the angle between the ligaments. The structures with a lower stiffness and a bigger angle between the ligaments (visualised with a θ in Figure 2.10) are more prone to buckling under compression and will show auxetic behavior (33).

The second structure is a re-entrant honeycomb structure with initial curved ligaments. It exhibits auxetic behavior because the curved ligaments will buckle under an applied load (29; 32). The auxetic value can be tuned by using an hierarchical system which also allows the material to be auxetic under compression and tension (29). If hierarchy is not applied, a material with a 180° curvature, as seen in the example in Figure 2.9d, will show auxetic behavior for tension as well as compression (32).

The third and final rectangular auxetic structure is the Miura-ori fold (35; 34). Within origami, the fold lines of the material are the ligaments. Whereas the previous two structures are based on the buckling of the ligaments, the ligaments of a Miura-ori fold are stiff and will stack upon each other under compression in one direction. This causes the Miura-ori fold to be relatively stiffer than the other two rectangular auxetic structures. A kirigami structure of a Miura-ori fold may be stiffer or more flexible than the origami variation depending on the fold angles (30). Otherwise, the kirigami equivalent show the same auxetic behavior (30; 36)

All discussed mechanical metamaterial have a different value or range of auxetic values. The values and ranges are visualised in Figure 2.11 and specified per paper.

Zero Poisson's ratio

A few metamaterials reviewed within the rectangular section show a zero Poisson's ratio. One rectangular metamaterial design exhibits the zero Poisson's ratio functionality, which is visualised in Figure 2.12. The design is based the re-entrant honeycomb from Figure 2.9d and cut vertically in half. One half remains the same whilst the other is reversed. A combination of the two halves will create a zero Poisson's ratio under applied loading because the deformation of each will cancel each other out (32). A similar design but slightly different, is when one of the two halves has a higher Young's modulus. This creates that the ligaments will buckle under an applied load whilst the other does not, thus creating a zero Poisson's ratio (37).

Stress distribution

Curving the ligaments of the metamaterial structure allows for a better stress distribution compared to structures with straight ligaments. An example of a better stress distribution is shown in the case for the curved ligament variations of the regular honeycomb and the re-entrant honeycomb (31; 32; 37). The load-displacement curve is (almost) linear for straight ligaments but non-linear for curved ligaments. The load-displacement relation of a straight ligament shows that the stiffness of a straight ligament might be greater during deformation because the stiffness will be a constant value. However, the stiffness of a curved ligaments is not constant and might sustain more deformations (31). The non-linear behavior of a curved ligament allows for a better stress distribution, with up to a 40% decrease in stress concentration compared to its straight ligament counterpart (32)(37). Furthermore, a lower stress distribution limits the plastic deformation (31).

In origami and kirigami, replacing the straight ligaments (the fold lines) with curved ligaments is not possible. A possible method for reducing the stress concentration in origami is by smoothing the transitions from facet to fold line (38). This method can be applied in kirigami as well. Additionally, adjusting the shape of the cuts or adding extra

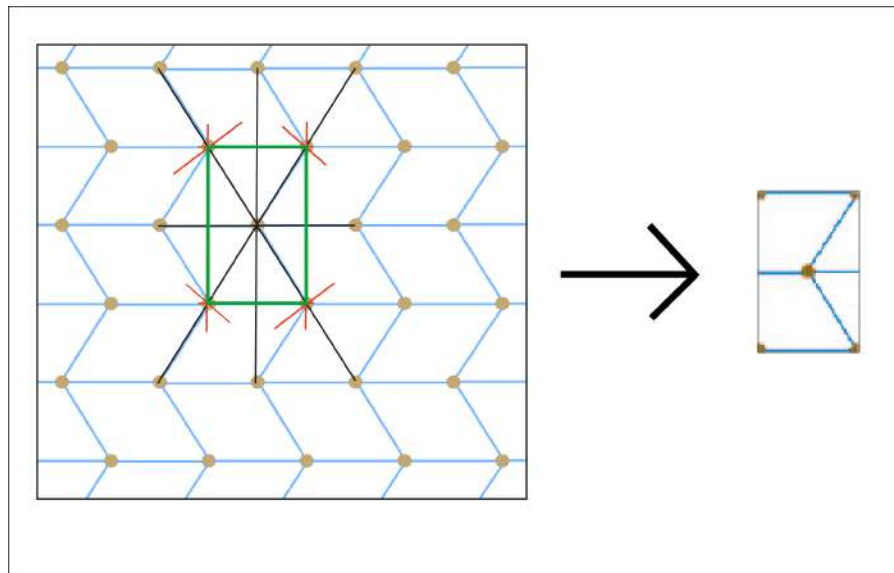


Figure 2.10: The Wigner-Seitz cell construction of the primitive unit cell of a zig-zag pattern. The yellow dots are the nodes that connect the blue ligaments. The black lines connect one lattice point to the neighbouring lattice points, afterwards which red lines are placed orthogonally. Finally, the intersection of the orthogonal lines creates the rectangular primitive unit cell illustrated in green. On the right side, the resulting rectangular unit cell is placed.

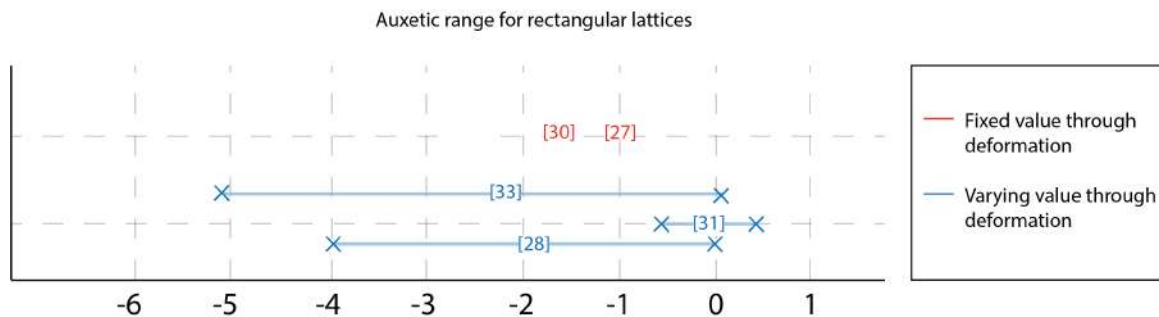


Figure 2.11: Overview of the auxetic range from papers reviewed in the rectangular section. In red are the papers mentioned which have a fixed value throughout the deformation. Papers which had a design that has a varying Poisson's ratio during deformation are depicted in a blue line with crosses at the lower and upper bound

folds along the hinge line are also a plausible method for stress reduction in kirigami (36). The stress distribution over the mechanical metamaterial structure can be modified by adjusting the parameter ratio of the unit cell height and length or by varying the thickness of the ligaments throughout the structure. If the thickness is uniform over all unit cells, the stress distribution is even(37).

Multi-stability

In order to create multi-stability, a non-linear behavior needs to be established. An element with negative stiffness has non-linear deformation behavior. Thus multi-stability can be created by integrating negative stiffness component. Most often, a negative stiffness component will buckle under an applied load. When a buckling mechanism is put in series with another buckling mechanism, one will be a bearing segment and the other the snapping segment which can create a multi-stable material because the two segments will buckle separately from each other under deformation (37).

In origami structure there are two methods in which the branch of motion can be made non-linear. The relation between the angle of the folds can make the force-displacement relation non-linear and thus multi-stable (39). Another possibility could be to halt the folding motion at a desired angle with a self-locking technique. A self-locking mechanism is achieved by varying the unit cell geometry between each column of a grid of origami unit cells. When a compressive force is applied the middle column will fold first. Under further compression the next adjoining columns will begin to fold. This creates a non-continuous folding motion (35).

Shape fitting

Another quality of the Miura-ori fold is that the initial planar configuration can be made into any desired shape whilst the folding motion is preserved (35). However, the rigid planes limit the Miura-ori fold in the number of out-of-plane shape during deformation. For a Miura-ori fold it is known that it has two deformation shapes: saddle and twisting

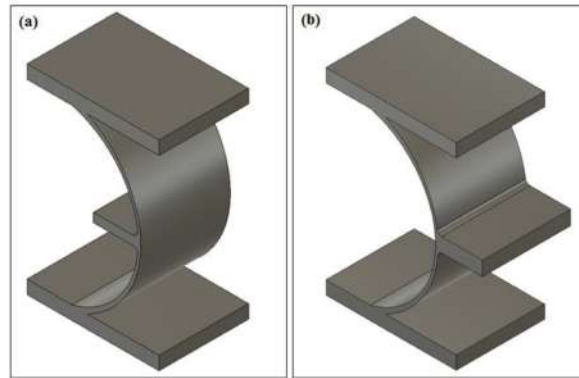


Figure 2.12: A negative and positive curved element which together form a zero Poisson's ratio element (32)

mode (35). The kirigami materials on the other hand show a greater versatility to fit to multiple shapes in its out-of-plane deformation. A kirigami cut that is especially known for its shape fitting is the fractal-cut. It is based on rotating units and can be made into a hierarchical structure. This makes the stretchability of the material remarkably high and allows for the shape fitting property (36).

The straight cuts and curved cuts have similar stretchability but the tensile strain of the curve-cut is slightly larger which is caused by the buckling modes of the ligaments (36).

Rectangular overview

All internal structures of the rectangular lattice category are either a zig-zag pattern, a re-entrant honeycomb or the Miura-ori sheet. Each of these internal structures have shown to be auxetic, but the some of the internal structures can have a zero Poisson's ratio with little adjustment. As is the case for a re-entrant honeycomb with curved ligaments. Using curved ligaments is in general a good method to improve the stress distribution under deformation. Additionally, incorporating curved ligaments in the internal structure of a mechanical metamaterial will make it multi-stable. The functionalities stress distribution, multi-stability and negative stiffness are a result of the force-displacement relation of a curved ligament being non-linear.

For the Miura-ori and kirigami configurations, the functionalities stress distribution and multi-stability are achieved in a different manner. Both functionalities are realized by tuning the geometrical parameters of the Miura-ori fold. A kirigami pattern has the added functionality of being shape fitting because a kirigami pattern is highly stretchable.

4.3. Square lattice

The third Bravais lattice group is the square lattice. As opposed to the rectangular lattice, the length of square lattice vectors are equal, $a = b$. The angle between the lattice vectors is still $\phi = 90^\circ$. In Figure 2.13, two lattice points grids (the black dots) are visualised which will create a square primitive unit cell when a Wigner-Seitz cell is constructed. Examples of structural designs that have a square primitive unit cell, are seen in Figure 2.14.

Five functionalities were found within the square Bravais lattice designs: auxetic (40; 24; 41; 42; 43; 44; 45; 46; 19), zero Poisson's ratio (47; 43; 45), stress distribution (43; 48), bi-stability (49) and shape fitting(36; 48; 24).

Auxetic

The auxetic square lattice has a rotating squares structure or a chiral-structure. One paper is reviewed which shows a mechanical metamaterial based on the re-entrant honeycomb. First, we look into the mechanical metamaterials that have a rotating squares structure. The basic principle of rotating squares is that it is a deformation mechanism in which square units are connected at their corners with hinges, see Figure 2.14a (40; 24; 41). A rotating squares mechanism shows a Poisson's ratio equal to -1 under tension. Notable is that the tension can be applied from any side (40). By using a hierarchical approach, the auxeticity becomes tunable. An example of a hierarchical approach is shown in Figure 2.14b. However, it must be noted that a too large deformation, i.e. a large angle between the square units, causes the Poisson's ratio to become positive (24).

In a rotating square structure, the square units are divided by a fractal cut. If a fractal cut is increased to, for example, a circular perforation, the metamaterial structure will become a perforated sheet. Whereas a rotating squares structure is auxetic under tension, a perforated sheet is auxetic under compression. The size of the perforations affects how much space there is for the material to deform under compression. The shape of this perforation could be rectangular (43), circular (44) or a combination of both in the form of a peanut (42). The peanut-shaped perforation shows a higher absolute auxetic value than the other perforated sheet materials (42). A mechanical metamaterial has a lower density when the perforations are bigger, and a higher density with smaller perforations. A higher density results in a Poisson's ratio closer to zero and could result in a Poisson's ratio of zero. A lower density results in a faster decrease in the Poisson's ratio and requires a lower force for deformation (43; 44).

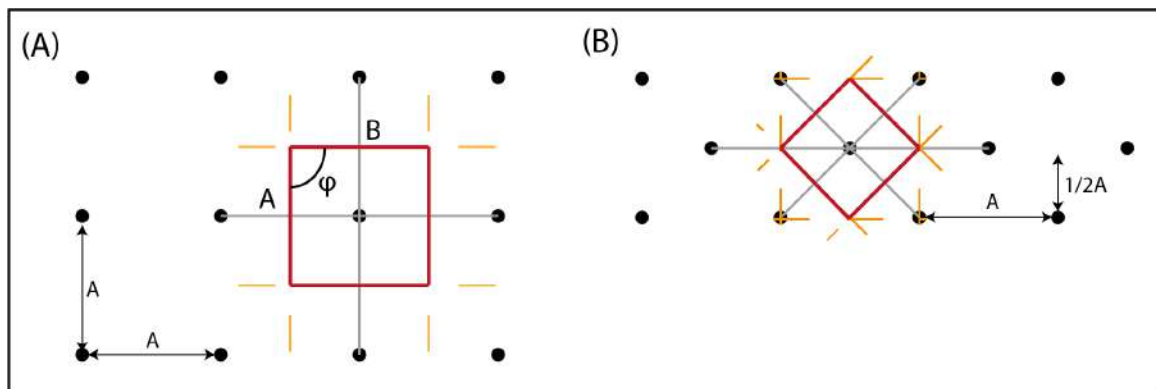


Figure 2.13: Two lattice point grid configurations the resulting primitive unit cell. The construction of the Bravais lattice is done according to the Wigner-Seitz cell method. The block dots represent the lattice points. One central lattice point is chosen and is connected to the neighbouring lattice point which is visualised with grey lines. An orthogonal yellow line is placed at the center of the grey line. The intersection of the yellow lines then provide the Bravais lattice in red lines. In general, lattice points that have an equal distance between them horizontally and vertically, and are stacked directly above each other, will give a square primitive cell (A). There is one exception to this, which is when the vertical distance is the half of the horizontal distance. If that is the case, then the primitive cell will also be square (B).

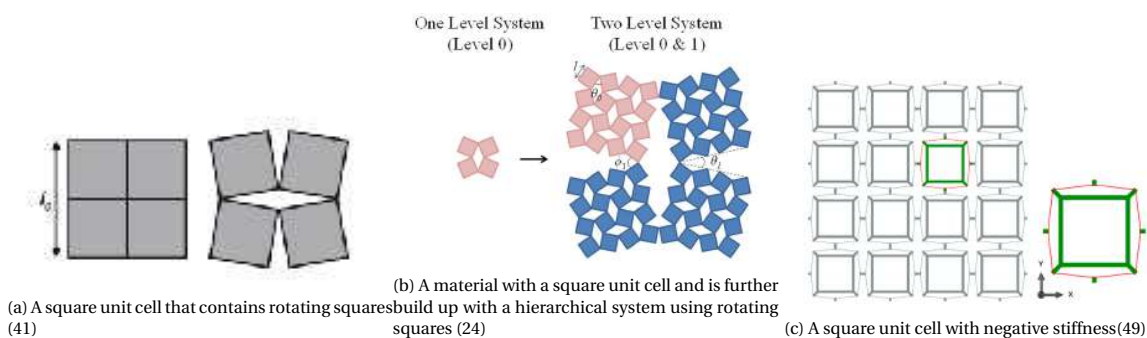


Figure 2.14: Three examples of square unit cells which vary in their internal structure

Next, we look at the tetra-chiral lattice structures. The nomenclature and mechanism of a chiral lattice has been explained in subsection 3.1. Both the tetra-chiral and the anti-tetra-chiral have a Poisson's ratio of $\nu = -1$ for a large range of geometrical parameter values. Do note that the Poisson's ratio of the tetra-chiral lattice varies with the ratio between the ligament thickness and node radius (19). The node can be made less rigid by removing it and allowing the ligaments to cross each other and create a star (46).

The final structure that is reviewed is the curved re-entrant honeycomb structure. In (Wang, 2022) (45) a design based on the re-entrant honeycomb with arc-shaped ligaments is introduced. Depending on the angle of the arc, the Poisson's ratio can be tuned. A smaller angle results in a smaller absolute auxetic value whereas a larger angle results in a larger absolute auxetic value. However, the material with the larger angle has a discontinuous Poisson's ratio development during deformation and quickly jumps to a higher Poisson's ratio. Due to a switch in bending and stretching deformation of the arc-shape ligaments, the Poisson's ratio varies throughout deformation.

An overview of the full auxetic range for every discussed paper with a square unit cell can be seen in Figure 2.15.

Zero Poisson's ratio

The rotating squares mechanism also has the ability to exhibit a Poisson's ratio of zero (47). Other than the auxetic rotating squares materials, this variation has the cuts placed differently. The difference is visualised in Figure 2.16. A perforated sheet can also have a zero Poisson's ratio by carefully selecting the material density (43).

In the curved ligament structure, the number of arcs on the ligament determines how the material deforms under an applied load. When there are multiple arcs along the axis perpendicular to the pulling force, the material has a Poisson's ratio almost equal to zero (45).

Stress distribution

Any type of perforation, may it be a fractal cut or a circular hole, induces a stress concentration at the edges of the perforation. Having the perforations closer to each other, i.e. a lower material density, the stress concentrations will be amplified (43). Adding a curvature to the edge of the perforation could lower the stress level. This could explain why peanut-shape perforation has a lower stress level compared to its elliptical counterpart (42). However, this is not explicitly stated in the paper.

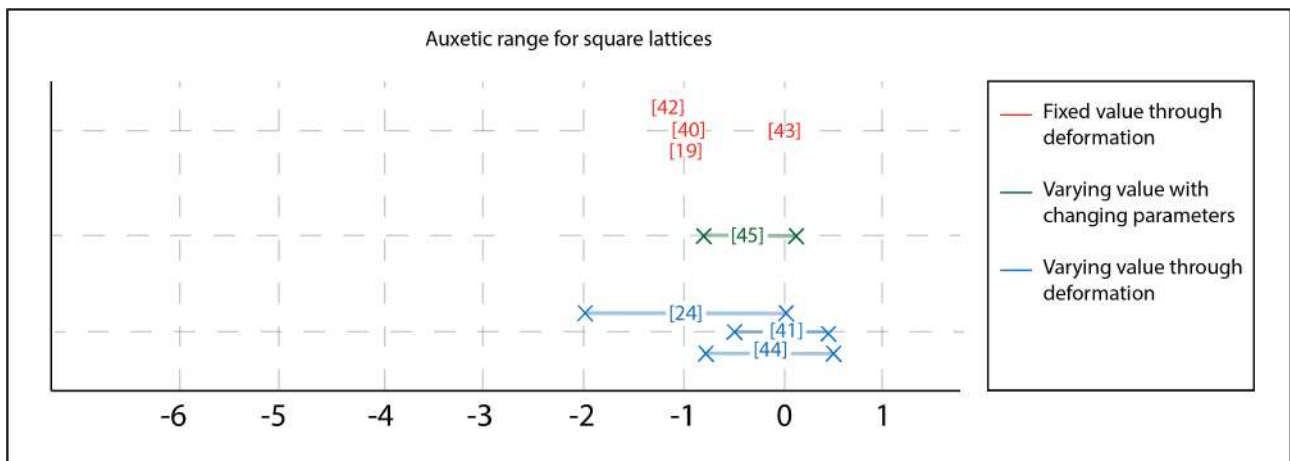


Figure 2.15: Overview of the auxetic papers within the square geometrical category. The paper citation colored in red have a fixed value during deformation. The papers noted in green have a varying Poisson's ratio due to a change in parameters. The papers noted in blue have a Poisson's ratio that varies during the deformation

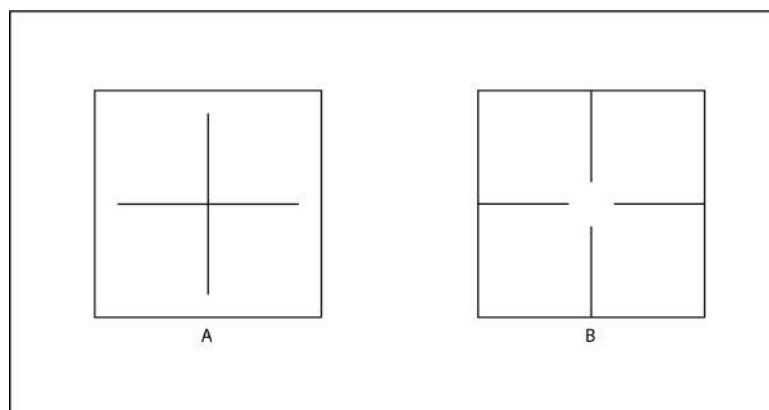


Figure 2.16: Two square lattices with A) having the fractal cuts placed to achieve a zero Poisson's ratio and B) having the cuts placed for auxetic behavior

Bi-stability

Equivalent to the results of the rectangular mechanical metamaterials, Figure 4.2, curved ligaments have a negative stiffness behavior during deformation (49; 50). A specific square unit cell that was reviewed, has curved ligaments on each side and a rigid square frame in the center, which can be seen in Figure 2.14c (49; 50). A rigid square frame provides the necessary boundary conditions in order for the curved ligaments to buckle under compression. If the square frame is not rigid enough, the deformation will be caused by rotation of the squares. When the ligaments buckle, the mechanical metamaterial will be multi-stable.

Shape fitting

Materials that show a large strain range are known to be shape fitting onto many surfaces. A material with fractal cuts can achieve large strains which otherwise would not have been able to achieve, which is seen in mechanical metamaterials with a rotating square mechanism (36). By adding hierarchy to the rotating squares mechanism, the stretching area can become even larger (24). This is done by dividing one square units into smaller square units, see Figure 2.14b. The number of degrees of freedom grows as the level of hierarchy increases. A hierarchical rotating squares mechanism is able to stretch up to 800% of its original area (48).

Square overview

The main internal structure in the square unit cells are chiral structures or rotating squares mechanism. The chiral structure only has the auxetic functionality in the reviewed papers. The square mechanism is in its basic variant auxetic but can have a zero Poisson's ratio when the fractal cuts are placed differently. Additionally, the rotating square mechanism is very stretchable and thus a good structure for shape fitting functionalities. When a hierarchical structure is applied to the rotating squares structure, the stretchability becomes larger.

A good stress distribution is difficult to achieve within the reviewed square Bravais lattice designs as only one paper specifically mentioned that the stated design lowered the stress concentrations. Next, a bi-stable mechanism is also reviewed only once. The bi-stable structure uses curved ligaments to enable negative stiffness behavior which results in a bi-stable structure.

4.4. Hexagonal lattice

The fourth and final Bravais lattice is the hexagonal lattice. It does not have fixed lattice vector dimensions, $a = b$ or $a \neq b$ are both possible, the angle between the lattice vectors is not perpendicular but larger, $\phi > 90^\circ$ (28). The corresponding lattice point grid configuration that will result in a hexagonal Wigner-Seitz cell is seen in Figure 2.17. The following six functionalities were found within the hexagonal Bravais lattice designs: auxetic (51; 19; 46; 52; 53; 47; 54; 55; 20), zero Poisson's ratio (56; 5; 57), stress distribution (20; 27), multi-stability (56; 6; 57) and shape reconfiguration (5; 6; 58).

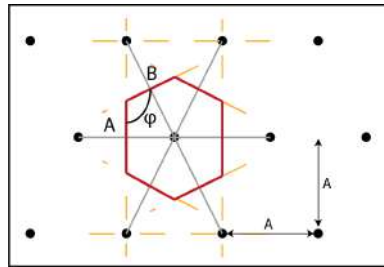


Figure 2.17: The lattice point grid configuration that results in a rectangular primitive unit cell. The construction of the Bravais lattice is done according to the Wigner-Seitz cell method. The block dots represent the lattice points. One central lattice point is chosen and is connected to the neighbouring lattice point which is visualised with grey lines. An orthogonal yellow line is placed at the center of the grey line. The intersection of the yellow lines then provide the Bravais lattice in red lines. When the lattice points are not stacked directly above each other, the primitive cell will be hexagonal. The horizontal and vertical distance may vary, the only exception is when the vertical distance is half of the horizontal distance because this will create a square primitive unit cell

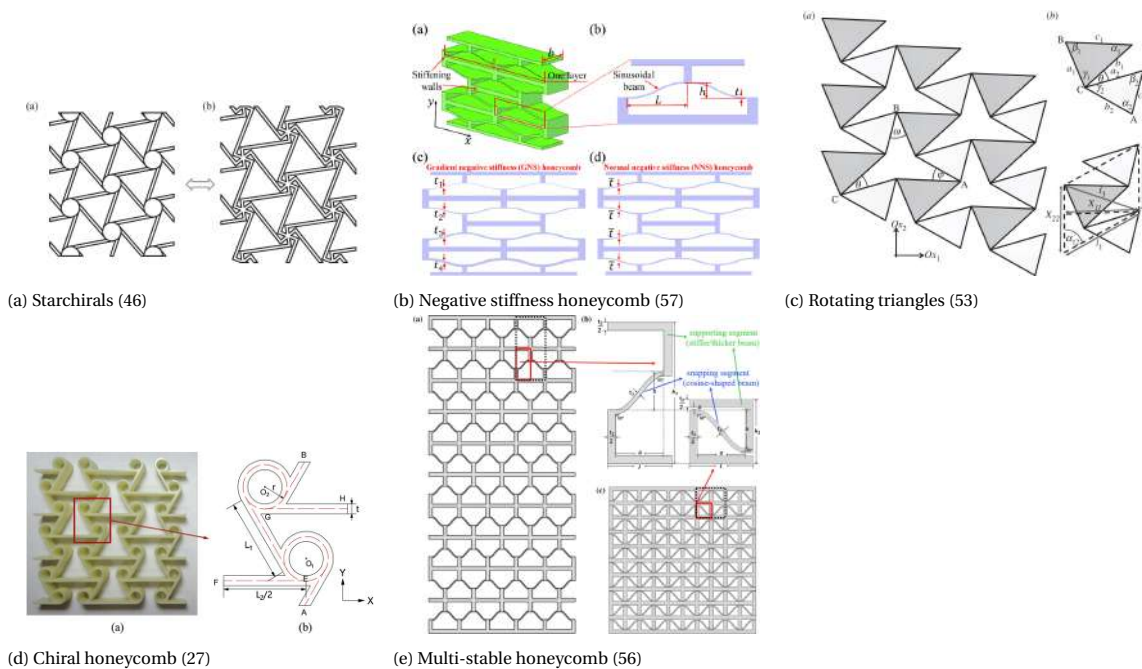


Figure 2.18: Examples of hexagonal unit cells

Auxetic

The Poisson's ratio ranges from $\nu = -4$ to $\nu = 0.9$ with one outlier that has the range $\nu = [-10 \quad 10]$. The details whether the Poisson's ratio of the design in a paper is constant or varying, can be seen in Figure 2.19. The auxetic structure that were found to have a hexagonal unit cell are the re-entrant honeycomb, chiral structures, rotating units and kirigami sheets.

When one thinks of a hexagonal pattern, the most immediate thought would be a honeycomb. A regular honeycomb can become auxetic under compression if the structure is made hierarchical and contains elastic instabilities in the connecting ligaments. Implementation of a (smaller) honeycomb at each corner of the main honeycomb, lowers the compressive strain such that the connecting ligaments can buckle during deformation. This material can then reach a negative Poisson's ratio during deformation (51). The added hierarchical order allows for auxetic behavior whereas a regular honeycomb, even with elastic instabilities, does not show auxeticity (59). Otherwise, the honeycomb can be made into its re-entrant version which yields auxetic behavior. The mechanical properties of a re-entrant honeycomb are mainly affected by the thickness of the ligaments (54).

Within the hexagonal Bravais lattice designs, there are two chiral variants. One has three ligaments (tri-chiral) connected to the node and the other has six (hexa-chiral). The stress-strain response for a chiral structure is linear, indicating that the Poisson's ratio is constant during deformation. Important to note is that the tri-chiral is not auxetic and the hexa-chiral is. This may be due to the Young's modulus of the material. A hexa-chiral structure has a relative high Young's modulus compared to a tri-chiral structure (19). The behavior of the anti-hexa-chiral is similar to that of a re-entrant honeycomb but the re-entrant honeycomb shows a larger auxetic range (achieving a more negative Poisson's ratio) and a similar stress accumulation compared to the chiral design (20). As the density of the material increases, the Young's modulus increases as well, which in turn causes a drop in the auxetic behavior (55).

Same as for the square auxetic section, the hexagonal design also contains a starchiral. A starchiral has two deformation mechanisms, bending of the ligaments between the nodes and bending of the ligaments in the nodes. An advantage of this design is that it allows for tuning of the Poisson's ratio (46).

A kagome lattice, also known as tri-hexagonal pattern, consists of a repetition of two triangles and two honeycombs meeting at one node (60). It has been studied as an actuation plate (61; 62), sandwich structure for a higher load bearing capacity (63; 64) and as an auxetic material (52; 53).

The kagome structure is auxetic if the triangles are solid planes because solid planes prevent the ligaments from deforming. The behavior is then similar to that of rotating squares in Figure 4.3, but instead of square units, the units are triangular. When the material is fully expanded, the pattern resembles a kagome pattern, a step in the expansion can be seen in Figure 2.18c. Similar to the rotating squares mechanism, the rotating triangles mechanism can reach a Poisson's ratio of $\nu = -1$. Interestingly, the Poisson's ratio of a rotating triangle material does not depend on the size of the triangles (triangles of which each ligament has the same dimension), the angle between them or the direction of applied force (52).

If the triangle units are made of two different sizes, the Poisson's ratio may be either positive or negative. During deformation of the material, when the angle between the triangles changes, the Poisson's ratio changes as well (53). The Poisson's ratio becomes negative when the structure is at a locking angle, i.e. the sum of the angle between the triangle and the angle between the ligaments of the triangle is equal to 180° . This applies for an applied force in one direction. In (Grima,2006) (52) it is already shown that a $[a \ a \ a] \times [a \ a \ a]$ triangle pair results in a constant negative Poisson's ratio. Next, (Grima,2012) (53) shows that a constant negative Poisson's ratio may also be obtained from $[a \ b \ c] \times [k \cdot a \ k \cdot b \ k \cdot c]$ triangle pair.

Lastly, kirigami sheets are included in the hexagonal Bravais lattice category. Assuming a rigid unit in a honeycomb shape and applying fractal cuts along the edges, the material can reach an auxetic behavior of $\nu = -3$ under tension. It is extremely stretchable and auxetic over a large range of deformation. A hexagonal kirigami material can either deform according to rotating units topology but can also deform according to bending ligaments. The rotating units mechanism is more applicable for smaller perforations, which are the fractal cuts. Material that deforms according to the bending of ligaments has a higher effective Young's modulus (47).

Zero Poisson's ratio

All reviewed hexagonal Bravais lattice designs that have a zero Poisson's ratio contain the negative stiffness honeycomb structure, as seen in Figure 2.18b. Note that the zero Poisson's ratio property is often not specifically stated in the papers. A negative stiffness honeycomb contains curved ligaments which are placed orthogonal to the loading direction.

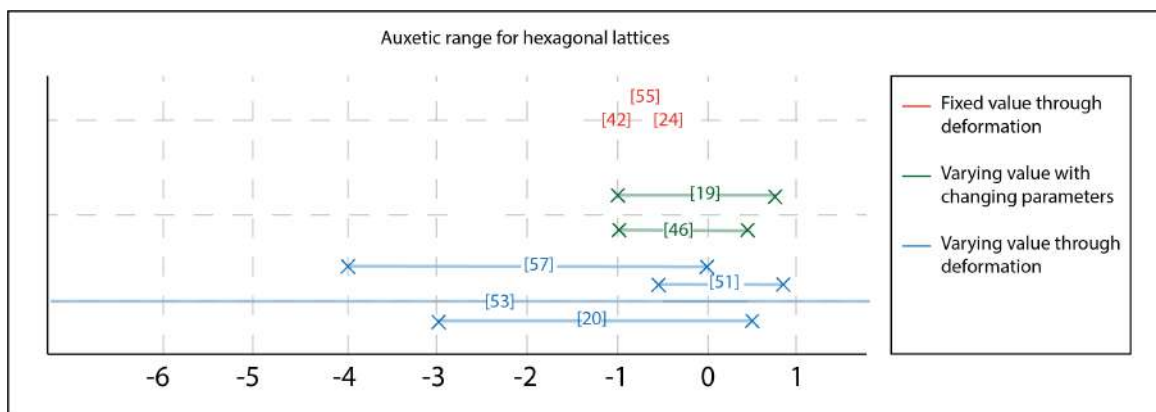


Figure 2.19: Auxetic range of hexagonal unit cell and specified paper references in brackets

The curved ligaments will buckle when a load is applied, whilst the parallel placed ligament functions as supporting ligaments. The curved ligaments buckle from one curvature to the other, thus they do not expand axially causing the material to have a zero Poisson's ratio (56; 5; 57).

Stress distribution

Within the hexagonal materials, the chiral materials and the kirigami sheets are the most applicable for a better stress distribution (20; 27). As stated in the Section 4.2, curved ligaments allow for a better stress distribution than its straight ligament counterparts. This is shown again by a chiral re-entrant honeycomb having a lower stress level than its regular re-entrant honeycomb counterpart. The maximum stress a chiral material can bear is dependent on its geometrical parameters. The cell-wall thickness will increase the maximum stress, whereas the ligament-length ratio will cause it to decrease (20).

Bi-/Multi-stability

The hexagonal Bravais lattice structures that exhibit multi-stability are based on buckling elements, similar to the structures in Figure 4.2 and Figure 4.3. Curved ligaments in a (re-entrant) honeycomb structure show bistable behavior due to snap-through behavior (6), such as the structure in Figure 2.18b. Whether the negative stiffness behavior is present, depends on the parameters of the curved ligament. The important parameters are either the ratio between the snapping segment and supporting segment thickness, or between the curve amplitude and length (56). For both parameter ratios applies that a low ratio does not result in the negative stiffness behavior and a higher ratio does although the mechanical metamaterial is not self-locking. An even higher ratio does result in self-locking mechanism and the structure becomes thus bistable (56; 6). The number of unit cell (a unit cell contains one hexagonal negative stiffness honeycomb) columns is associated with the maximum required force. The relation is linear, a doubling of the columns leads to a doubling of the maximum force (6). The negative stiffness honeycomb can become multi-stable with a gradient property is applied. By varying the thickness of the curved ligaments, each row has a different force threshold for buckling. The incremental increase in thickness causes a similar incremental increase in the required buckling force, thus creating a multi-stable mechanical metamaterial (56; 57).

Shape reconfiguration

When a second curved ligament is added to a negative stiffness honeycomb, the mechanical metamaterial will not be bi-stable anymore. This is a result of the curved ligaments not being self-locking anymore. Both will never fully buckle to the second stable state as there is not enough room. These materials have the functionality to reconfigure to their original shape (5; 6; 58).

Hexagonal overview

The hexagonal Bravais lattice category has shown to have many structure variations to be auxetic: chiral designs, rotating unit (resembled in a Kagome pattern) and kirigami designs. The chiral and kirigami designs also have a good stress distribution. The auxetic structures are, however, not the designs that also contain a zero Poisson's ratio. To obtain a zero Poisson's ratio with a hexagonal unit cell, a re-entrant honeycomb with curved ligaments is used. This configuration is also mostly used to have a negative stiffness behavior and multi-stability. Furthermore, two parallel placed curved ligaments allow the mechanical metamaterial to reconfigure to its original shape after a force has been applied.

5. Discussion

The Bravais lattice categorization that was set up for this literature review, allowed all the reviewed papers to be categorized according to the shape of the primitive unit cell. A small difference is seen in the number of papers reviewed per Bravais lattice category. The majority of the reviewed papers fall into the hexagonal category. This may be due to a self-amplification of the honeycomb pattern being most often researched and thus again containing more iterations of those designs. Another possibility could be that a hexagonal unit cell allows for more variations within its structure than the other Bravais lattice unit cells. This is supported by Gruebler's formula that calculates the Degrees of Freedom (DoF) for a mechanism (65). The Gruebler formula shows that a hexagonal lattice structure has the possibility to possess more DoF than the other categories because a hexagonal lattice has six moving ligaments whereas a square or rectangular lattice has four moving ligaments.

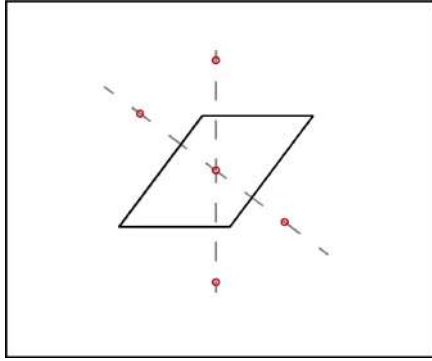
Interestingly, there were no papers analyzed that fit into the oblique lattice category. Although some mechanical metamaterials have oblique angles within their structure, their primitive unit cell are not oblique lattices. It must be noted that oblique unit cells do occur in 3D configurations (66), but for this literature study, no 2D configurations of the oblique unit cell were found. This raises the question as to whether, for example, an oblique unit cell is possible or whether this is physically impossible.

5.1. Oblique lattice

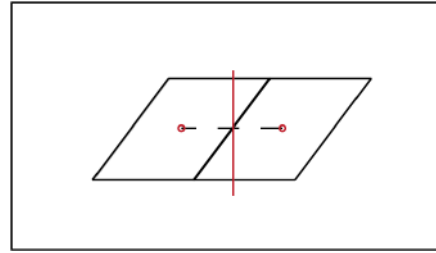
The primitive unit cells in this literature review are determined with the Wigner-Seitz method. To determine whether it is physically possible to construct an oblique Wigner-Seitz cell, let's try to investigate what the possible lattice point

structure of an oblique lattice might be. First, we assume an oblique Wigner-Seitz cell and deconstruct it. In Figure 2.20a, an oblique primitive cell is shown with the possible lattice points (red circles) of an oblique grid. If one were to copy and paste this, the red circles would show the grid. However, by copy and pasting this unit cell once, see Figure 2.20b, it can already be seen that an oblique grid is not possible. One oblique lattice copy shows that the center lattice point already creates a lattice vector (shown in red) that does not coincide with the oblique lattice.

Although the Bravais lattice categorization captures all constructed primitive unit cells, one category will remain empty when the Wigner-Seitz method is used. As previously stated, Bravais lattices were chosen as a categorization because they describe every shape that can fill a plane. To the authors knowledge there is not another unit cell categorization that has this property. Therefore, using the Bravais lattice as a categorization reference looks the most compatible.



(a) An oblique unit cell (black lines) deconstructed according to the Wigner-Seitz method. The dotted black lines are the construction lines that connect two lattice points, which are visualized with red circles.



(b) Two oblique unit cells next to each other. By connecting their center lattice points with a construction line (black dotted line), the lattice vector can be constructed (red line). This lattice vector does not coincide with the original black lines of the oblique unit cell.

Figure 2.20: Two figures which together describe whether an oblique lattice is possible with a Wigner-Seitz cell.

For the rest of this discussion, when it is stated that something occurs in every geometrical category, it includes the categories rectangular, square and hexagonal lattice.

5.2. Auxetic

The auxetic property is the most researched and found property for every geometrical category. The Poisson's ratio range of each the geometrical category is almost the same, albeit that the hexagonal category differs slightly, see Figure 2.21. However, it must be noted that one hexagonal design is left out because its auxetic range is $\nu = [-10 \ 10]$, which is a much larger range than that of the other designs. Out of the 45 papers, 25 were on auxetic behavior. It is a property that has been studied widely, which is illustrated by there being several reviews on auxetic mechanical metamaterials (67; 7; 68; 69) and only one comparable review for non-auxetic materials (70). The first mention of an auxetic two-dimensional material in literature is the re-entrant honeycomb (71). This paper is the base for most following papers on auxetic metamaterials and thus explains the possible self-amplification that the auxetic hexagonal metamaterial is a big category in this literature review.

The auxetic range for every geometrical category is laid out in Figure 2.21. Even though the auxetic property is found in every geometrical category, the method to reach auxetic behavior is not the same. Three different methods are distinguished:

- Buckling instabilities: rectangular, square and hexagonal Bravais lattices.
- Rotating units: square and hexagonal Bravais lattices.
- Chiral structures: square and hexagonal Bravais lattices.

One method is applied every section, containing buckling instabilities in the structural design is one of them. Most often it is found in the form of a re-entrant honeycomb with curved ligaments along the orthogonal axis of the applied force. The curved ligaments generate buckling instabilities within the mechanism. In general, this method is based on tension, however, a rectangular configuration is reviewed which is based on compression. The curved ligaments that are usually bent inwards, as seen in Figure 2.9d, are bended outwards in the rectangular configuration, as seen in the zoom-in in Figure 2.9a. Besides the direction of the applied force, there are no discrepancies. Continuing on design with elastic instabilities: in the rectangular category, the zig-zag pattern was found to be auxetic if the ligaments contain elastic instabilities. The rectangular configuration can be translated to a square configuration by adjusting the length of the ligaments. Shorter ligaments in one direction will result in a square primitive unit cell when the Wigner-Seitz method is applied. A translation to the hexagonal category is also possible, as long as the ligaments parallel to the applied force are stiff enough to not buckle.

The second reviewed method is that of the rotating units. These are, in its most basic form, units connected with a simple joint at the corners and usually have a Poisson's ratio of $\nu = -1$. A perfect rotating joint at the corner of a compliant design is more so theoretical, in practice this method is only seen in the kirigami designs. The Poisson's ratio can be tuned by introducing hierarchy, which is observed in the square lattice group. The hierarchy in the rotating square mechanism is incorporated by cutting a square into four new squares. Applying hierarchy to a rotating unit mechanism is not discussed in the other categories. However, a triangle can be cut into multiple smaller triangles and a rectangle can be cut into multiple rectangles, indicating that hierarchy in rotating units is not exclusive for a square unit, the same principle can be applied to a rectangular or a hexagonal rotating unit. Additional papers that elaborate on hierarchy in rectangular or hexagonal rotating units were not found by the author. The principle of rotating units is further expanded to perforated sheets and kagome structures, found in square lattices and hexagonal lattices respectively. Perforated sheets ensure a larger range of auxeticity. The kagome structure is exclusive for the hexagonal lattice due to its basic configuration.

The last overlapping method is the chiral method which is within both the square and the hexagonal unit cell. Besides the difference in the number of connected ligaments, there is little difference in parameter design. For both geometrical categories, the same parameters have an influence on the Poisson's ratio.

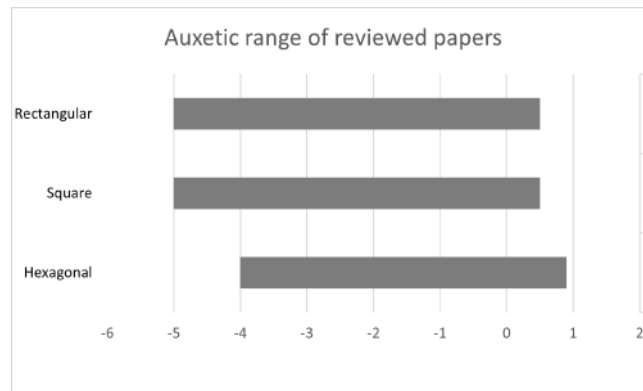


Figure 2.21: Auxetic range per category of reviewed papers

5.3. Zero Poisson's ratio

Research has been conducted in making the Poisson's ratio tunable. This leads to mechanical metamaterials with a zero Poisson's ratio and is observed in every geometrical category. Similar as to obtaining auxetic behavior, a structure with a zero Poisson's ratio is often inspired by the honeycomb configuration. The structures that have a zero Poisson's ratio make use of various combinations of curved ligaments, i.e. two parallel curved ligaments or multiple curvatures in one ligaments.

The square geometrical category uses one other method, namely the rotating units method. This could indicate that possible rotating rectangles or hexagons may also have a zero Poisson's ratio. However, papers that contain rotating rectangles or hexagons and showed a zero Poisson's ratio, were not found by the author. Using the rotating unit mechanism to create a zero Poisson's ratio was furthermore applied in perforated sheets. In the perforated sheets the property is obtained by increasing the material density which enables to halt the deformation at the desired point and create a zero Poisson's ratio.

5.4. Stress distribution

Within the geometrical categories, the methods that are used to reduce stress concentrations are all based on the same principle. In general, curved ligaments or rounded corners lower the stress concentration of a mechanical metamaterial during deformation. Sharp corners and straight ligaments are not the most suited for a good stress distribution. In origami structures, a curved ligament is not possible but it is possible to smooth a sharp fold which will lower the stress concentration. Thus, adjusting a part that contains sharp edges or is straight to containing curvatures or round edges, will enhance the stress distribution of the material.

5.5. Multi-stability

Whether a mechanical metamaterial is multi-stable, depends on the force-displacement relation. If the curve of the relation is non-linear and contains a part with a negative slope, then multiple local optima on the curve are possible, which are the stable positions of the material. Most internal structure use curved ligaments to obtain multi-stability. A curved ligament has an elastic instability and is has thus a non-linear behavior. Structures with curved ligaments are found in all geometrical categories. The elastic instability is achieved by applying a force perpendicular to a curved ligament which brings the structure from one stable state to the next stable state.

The basic idea of having negative stiffness behavior in a material is alluring. However, in reality, buckling is an unstable deformation mechanism (25). It is interesting to combine a negative stiffness component with a positive stiffness component. Such a combination placed parallel could result in a zero-stiffness mechanism, like (Hoetmer,2010) (12) demonstrated.

There is a difference between the geometrical section in terms of the direction of the applied force. The square unit cell is bi-directional, meaning that the force can be applied from any side. It can be seen as an expansion from the uni-directional unit cells from the rectangular and hexagonal category, which have curved ligaments placed only along one direction. A bi-directional unit cell has curved ligaments placed along both axes. This principle can be applied to the other categories as well.

The hexagonal unit cell also shows that it can have a gradient property which allows for tuning of the number of stable states. This same method could also be applied to the materials in the rectangular and the square category.

Origami designs were only found in the Section 4.3. However, the discussed papers did not contain multi-stability. It can be achieved by introducing non-linearity in the force-displacement relation.

5.6. Shape reconfiguration

Shape reconfiguration is a property which only explicitly appears in the reviewed papers for the hexagonal geometrical section. The shape reconfiguration is based on two parallel curved ligaments which prevents the ligament to buckle and thus never reach the second stable state and reconfigure to its original shape. Using a curved ligament stems from a design that is often used to obtain negative stiffness which is most often found in the hexagonal category but also a few designs in the rectangular and square Bravais lattice category. It seems that a snowball effect is the cause as to why the integration of a second parallel curved ligament is only applied in the hexagonal category. However, this is not the reason why shape reconfiguration is not found in the square and rectangular category because the principle can be applied to the multi-stable materials from those categories. It must be noted that doing this eliminates the negative stiffness behavior. Next, it must also be noted that not all designs that contain negative stiffness in this literature review have the space to add a second curved ligament.

5.7. Shape fitting

Shape fitting is a property that is found in the rectangular and square category. In both cases it is based on the kirigami principle. Due to it being based on rotating units, the stretchability of the material is very high. This is not a method that is exclusively for rectangular and square unit cells. By ensuring that the unit is a hexagonal or triangular, the hexagonal Bravais lattice category can also incorporate shape fitting properties. Applying the kirigami method to a design with hexagonal or triangular unit is a bit less straight forward than it is for square and rectangular units. The fractal cuts in with a square or rectangular unit are parallel or orthogonal to each other, whereas with a hexagonal or triangular unit the fractal cuts are placed in a more complex fashion.

6. Conclusion

Mechanical metamaterials have been researched extensively in the recent decades. However, application experiments are missing. An interesting application would be to implement a mechanical metamaterial as a building block in shell mechanisms. To establish which mechanical metamaterials could be used, the following research question is stated: Which functionalities are exhibited by planar and elastic mechanical metamaterials?

The primitive unit cells of the reviewed mechanical metamaterials are made with the Wigner-Seitz method. Next, the resulting shapes are categorized according to the four 2D Bravais lattices. The functionalities that are exhibited by the mechanical metamaterials are classified as auxetic behavior, a zero Poisson's ratio, stress distribution, negative stiffness behavior, bi-/multi-stability, shape reconfiguration and shape fitting.

It is found that no papers have a design with a primitive unit cell that fits into the oblique lattice category. This is due to it not being possible to construct an oblique primitive cell with the Wigner-Seitz method. From the constructed primitive unit cells, most fall into the hexagonal geometrical category. Additionally, the most designs contain the auxetic functionality. Both can be a result of a re-entrant honeycomb being the first mentioned auxetic design causing an amplification of this specific design. This led to many more designs on the auxetic functionality and hexagonal designs.

Most functionalities are exhibited by the three geometrical categories rectangular, square and hexagonal. Except for shape reconfiguration and shape fitting which are only mentioned in the hexagonal and the square and rectangular papers respectively. There is not a physical reason why these functionalities are not exhibited within the other geometrical categories because the applied method to achieve either functionality can be translated to the desired Bravais lattice. The reason as to why there are no, for example, hexagonal papers reviewed with a shape fitting functionality is probably it is due to additional complexity. The other functionalities are mentioned in every geometrical category. The functionalities stress distribution, negative stiffness, shape reconfiguration and shape fitting each had one type of internal structure that led to their corresponding functionality. To reach the auxetic, zero Poisson's ratio or bi-/multi-stability, several internal structures were possible.

The next step will be to conduct application experiments or to expand the overview of this literature review, for

example by researching a hexagonal mechanical metamaterial that has the functionality to shape fit. The first step has been provided by this literature review such that the reader can choose which mechanical metamaterial is the best fit for their research.

Bibliography

- [1] A. A. Zadpoor, "Mechanical performance of additively manufactured meta-biomaterials," *Acta biomaterialia*, vol. 85, pp. 41–59, 2019.
- [2] S. A. Cummer, J. Christensen, and A. Alù, "Controlling sound with acoustic metamaterials," *Nature Reviews Materials*, vol. 1, no. 3, pp. 1–13, 2016.
- [3] C. M. Soukoulis and M. Wegener, "Past achievements and future challenges in the development of three-dimensional photonic metamaterials," *Nature photonics*, vol. 5, no. 9, pp. 523–530, 2011.
- [4] E. Barchiesi, M. Spagnuolo, and L. Placidi, "Mechanical metamaterials: a state of the art," *Mathematics and Mechanics of Solids*, vol. 24, no. 1, pp. 212–234, 2019.
- [5] D. A. Debeau, C. C. Seepersad, and M. R. Haberman, "Impact behavior of negative stiffness honeycomb materials," *Journal of Materials Research*, vol. 33, no. 3, pp. 290–299, 2018.
- [6] D. M. Correa, C. C. Seepersad, and M. R. Haberman, "Mechanical design of negative stiffness honeycomb materials," *Integrating Materials and Manufacturing Innovation*, vol. 4, no. 1, pp. 165–175, 2015.
- [7] X. Ren, R. Das, P. Tran, T. D. Ngo, and Y. M. Xie, "Auxetic metamaterials and structures: a review," *Smart materials and structures*, vol. 27, no. 2, p. 023001, 2018.
- [8] S. Adriaenssens, P. Block, D. Veenendaal, and C. Williams, *Shell structures for architecture: form finding and optimization*. Routledge, 2014.
- [9] K. A. Seffen, "Compliant shell mechanisms," *Philosophical Transactions of the Royal Society A: Mathematical, Physical and Engineering Sciences*, vol. 370, no. 1965, pp. 2010–2026, 2012.
- [10] E. Kebabdz, S. Guest, and S. Pellegrino, "Bistable prestressed shell structures," *International Journal of Solids and Structures*, vol. 41, no. 11-12, pp. 2801–2820, 2004.
- [11] S. Guest, E. Kebabdz, and S. Pellegrino, "A zero-stiffness elastic shell structure," *Journal of Mechanics of Materials and Structures*, vol. 6, no. 1, pp. 203–212, 2011.
- [12] K. Hoetmer, G. Woo, C. Kim, and J. Herder, "Negative stiffness building blocks for statically balanced compliant mechanisms: design and testing," 2010.
- [13] B. Lechthaler, C. Pauly, and F. Mücklich, "Objective homogeneity quantification of a periodic surface using the gini coefficient," *Scientific Reports*, vol. 10, no. 1, pp. 1–17, 2020.
- [14] Britannica, "Unit cell." <https://www.britannica.com/science/Bravais-lattice>. Accessed: 21-11-2022.
- [15] U. of cambridge, "Unit cell." https://www.doitpoms.ac.uk/tlplib/crystallography3/unit_cell.php. Accessed: 28-08-2022.
- [16] S. H. Simon, *The Oxford solid state basics*. OUP Oxford, 2013.
- [17] S. F. Kettle and L. J. Norrby, "The wigner-seitz unit cell," *Journal of Chemical Education*, vol. 71, no. 12, p. 1003, 1994.
- [18] H. da Motta, "Chirality and neutrinos, a student first approach," in *Journal of Physics: Conference Series*, vol. 1558, p. 012014, IOP Publishing, 2020.
- [19] A. Alderson, K. L. Alderson, D. Attard, K. E. Evans, R. Gatt, J. N. Grima, W. Miller, N. Ravirala, C. Smith, and K. Zied, "Elastic constants of 3-, 4-and 6-connected chiral and anti-chiral honeycombs subject to uniaxial in-plane loading," *Composites Science and Technology*, vol. 70, no. 7, pp. 1042–1048, 2010.
- [20] A. Alomarah, D. Ruan, S. Masood, I. Sbarski, and B. Faisal, "An investigation of in-plane tensile properties of re-entrant chiral auxetic structure," *The International Journal of Advanced Manufacturing Technology*, vol. 96, no. 5, pp. 2013–2029, 2018.
- [21] R. Lakes, "Materials with structural hierarchy," *Nature*, vol. 361, no. 6412, pp. 511–515, 1993.

- [22] J. U. Surjadi, L. Gao, H. Du, X. Li, X. Xiong, N. X. Fang, and Y. Lu, "Mechanical metamaterials and their engineering applications," *Advanced Engineering Materials*, vol. 21, no. 3, p. 1800864, 2019.
- [23] Y. Sun and N. M. Pugno, "In plane stiffness of multifunctional hierarchical honeycombs with negative poisson's ratio sub-structures," *Composite Structures*, vol. 106, pp. 681–689, 2013.
- [24] R. Gatt, L. Mizzi, J. I. Azzopardi, K. M. Azzopardi, D. Attard, A. Casha, J. Briffa, and J. N. Grima, "Hierarchical auxetic mechanical metamaterials," *Scientific reports*, vol. 5, no. 1, pp. 1–6, 2015.
- [25] E. Zurich, "Negative stiffness." <https://mm.ethz.ch/research-overview/material-modeling/negative-stiffness.html>. Accessed: 10-10-2022.
- [26] S. Palathingal and G. Ananthasuresh, "Design of bistable arches by determining critical points in the force-displacement characteristic," *Mechanism and Machine Theory*, vol. 117, p. Pages 175–188, 07 2017.
- [27] L. Hu, Z. Luo, Z. Zhang, M. Lian, and L. Huang, "Mechanical property of re-entrant anti-trichiral honeycombs under large deformation," *Composites Part B: Engineering*, vol. 163, pp. 107–120, 2019.
- [28] G. U. of Technology, "Two dimensional wigner-seitz cell." <https://lampx.tugraz.at/~hadley/ss1/problems/bravais/Q.php>. Accessed: 31-08-2022.
- [29] M. F. Berwind, A. Kamas, and C. Eberl, "A hierarchical programmable mechanical metamaterial unit cell showing metastable shape memory," *Advanced Engineering Materials*, vol. 20, no. 11, p. 1800771, 2018.
- [30] M. Eidini and G. H. Paulino, "Unraveling metamaterial properties in zigzag-base folded sheets," *Science advances*, vol. 1, no. 8, p. e1500224, 2015.
- [31] Y. Fu and W. Liu, "Design of mechanical metamaterial with controllable stiffness using curved beam unit cells," *Composite Structures*, vol. 258, p. 113195, 2021.
- [32] S. Gao, W. Liu, L. Zhang, and A. K. Gain, "A new polymer-based mechanical metamaterial with tailorable large negative poisson's ratios," *Polymers*, vol. 12, no. 7, p. 1492, 2020.
- [33] Z. Zhao, C. Yuan, M. Lei, L. Yang, Q. Zhang, H. Chen, H. J. Qi, and D. Fang, "Three-dimensionally printed mechanical metamaterials with thermally tunable auxetic behavior," *Physical Review Applied*, vol. 11, no. 4, p. 044074, 2019.
- [34] Z. Y. Wei, Z. V. Guo, L. Dudte, H. Y. Liang, and L. Mahadevan, "Geometric mechanics of periodic pleated origami," *Physical review letters*, vol. 110, no. 21, p. 215501, 2013.
- [35] M. Schenk and S. D. Guest, "Geometry of miura-folded metamaterials," *Proceedings of the National Academy of Sciences*, vol. 110, no. 9, pp. 3276–3281, 2013.
- [36] Y. Sun, W. Ye, Y. Chen, W. Fan, J. Feng, and P. Sareh, "Geometric design classification of kirigami-inspired metastructures and metamaterials," in *Structures*, vol. 33, pp. 3633–3643, Elsevier, 2021.
- [37] A. Rafsanjani, A. Akbarzadeh, and D. Pasini, "Snapping mechanical metamaterials under tension," *Advanced Materials*, vol. 27, no. 39, pp. 5931–5935, 2015.
- [38] H. Fang, S.-C. A. Chu, Y. Xia, and K.-W. Wang, "Programmable self-locking origami mechanical metamaterials," *Advanced Materials*, vol. 30, no. 15, p. 1706311, 2018.
- [39] S. Waitukaitis, R. Menaut, B. G.-g. Chen, and M. Van Hecke, "Origami multistability: From single vertices to metasheets," *Physical review letters*, vol. 114, no. 5, p. 055503, 2015.
- [40] J. N. Grima and K. E. Evans, "Auxetic behavior from rotating squares," 2000.
- [41] M. Sakovsky and P. Ermanni, "A thin-shell shape adaptable composite metamaterial," *Composite Structures*, vol. 246, p. 112390, 2020.
- [42] H. Wang, Y. Zhang, W. Lin, and Q.-H. Qin, "A novel two-dimensional mechanical metamaterial with negative poisson's ratio," *Computational Materials Science*, vol. 171, p. 109232, 2020.
- [43] A. Slann, W. White, F. Scarpa, K. Boba, and I. Farrow, "Cellular plates with auxetic rectangular perforations," *physica status solidi (b)*, vol. 252, no. 7, pp. 1533–1539, 2015.
- [44] K. Bertoldi, P. M. Reis, S. Willshaw, and T. Mullin, "Negative poisson's ratio behavior induced by an elastic instability," *Advanced materials*, vol. 22, no. 3, pp. 361–366, 2010.

- [45] M. Wang, H. Wu, L. Yang, A. Chen, P. Chen, H. Wang, Z. Chen, and C. Yan, "Structure design of arc-shaped auxetic metamaterials with tunable poisson's ratio," *Mechanics of Advanced Materials and Structures*, pp. 1–11, 2022.
- [46] D. Attard, P. Farrugia, R. Gatt, and J. Grima, "Starchirals—a novel class of auxetic hierarchal structures," *International Journal of Mechanical Sciences*, vol. 179, p. 105631, 2020.
- [47] L. Mizzi, E. Salvati, A. Spaggiari, J.-C. Tan, and A. M. Korsunsky, "Highly stretchable two-dimensional auxetic metamaterial sheets fabricated via direct-laser cutting," *International Journal of Mechanical Sciences*, vol. 167, p. 105242, 2020.
- [48] Y. Cho, J.-H. Shin, A. Costa, T. A. Kim, V. Kunin, J. Li, S. Y. Lee, S. Yang, H. N. Han, I.-S. Choi, *et al.*, "Engineering the shape and structure of materials by fractal cut," *Proceedings of the National Academy of Sciences*, vol. 111, no. 49, pp. 17390–17395, 2014.
- [49] C. Ren, D. Yang, and H. Qin, "Mechanical performance of multidirectional buckling-based negative stiffness metamaterials: an analytical and numerical study," *Materials*, vol. 11, no. 7, p. 1078, 2018.
- [50] T. Klatt and M. R. Haberman, "A nonlinear negative stiffness metamaterial unit cell and small-on-large multiscale material model," *Journal of Applied Physics*, vol. 114, no. 3, p. 033503, 2013.
- [51] D. Mousanezhad, S. Babae, H. Ebrahimi, R. Ghosh, A. S. Hamouda, K. Bertoldi, and A. Vaziri, "Hierarchical honeycomb auxetic metamaterials," *Scientific reports*, vol. 5, no. 1, pp. 1–8, 2015.
- [52] J. N. Grima and K. E. Evans, "Auxetic behavior from rotating triangles," *Journal of materials science*, vol. 41, no. 10, pp. 3193–3196, 2006.
- [53] J. N. Grima, E. Chetcuti, E. Manicaro, D. Attard, M. Camilleri, R. Gatt, and K. E. Evans, "On the auxetic properties of generic rotating rigid triangles," *Proceedings of the Royal Society A: Mathematical, Physical and Engineering Sciences*, vol. 468, no. 2139, pp. 810–830, 2012.
- [54] J. N. Grima, D. Attard, B. Ellul, and R. Gatt, "An improved analytical model for the elastic constants of auxetic and conventional hexagonal honeycombs," *Cellular Polymers*, vol. 30, no. 6, pp. 287–310, 2011.
- [55] T. Tancogne-Dejean, N. Karathanasopoulos, and D. Mohr, "Stiffness and strength of hexachiral honeycomb-like metamaterials," *Journal of Applied Mechanics*, vol. 86, no. 11, 2019.
- [56] H. Yang and L. Ma, "Multi-stable mechanical metamaterials by elastic buckling instability," *Journal of materials science*, vol. 54, no. 4, pp. 3509–3526, 2019.
- [57] S. Chen, X. Tan, J. Hu, S. Zhu, B. Wang, L. Wang, Y. Jin, and L. Wu, "A novel gradient negative stiffness honeycomb for recoverable energy absorption," *Composites Part B: Engineering*, vol. 215, p. 108745, 2021.
- [58] B. M. Goldsberry and M. R. Haberman, "Negative stiffness honeycombs as tunable elastic metamaterials," *Journal of applied physics*, vol. 123, no. 9, p. 091711, 2018.
- [59] B. Haghpanah, J. Papadopoulos, D. Mousanezhad, H. Nayeb-Hashemi, and A. Vaziri, "Buckling of regular, chiral and hierarchical honeycombs under a general macroscopic stress state," *Proceedings of the Royal Society A: Mathematical, Physical and Engineering Sciences*, vol. 470, no. 2167, p. 20130856, 2014.
- [60] M. Mekata, "Kagome: The story of the basketweave lattice," *Physics Today*, vol. 56, no. 2, p. 12, 2003.
- [61] A. Leung and S. Guest, "Single member actuation of kagome lattice structures," *Journal of Mechanics of Materials and Structures*, vol. 2, no. 2, pp. 303–317, 2007.
- [62] N. Wicks and S. Guest, "Single member actuation in large repetitive truss structures," *International Journal of Solids and Structures*, vol. 41, no. 3-4, pp. 965–978, 2004.
- [63] S. Hyun, A. M. Karlsson, S. Torquato, and A. Evans, "Simulated properties of kagomé and tetragonal truss core panels," *International Journal of Solids and Structures*, vol. 40, no. 25, pp. 6989–6998, 2003.
- [64] W. Wu, W. Hu, G. Qian, H. Liao, X. Xu, and F. Berto, "Mechanical design and multifunctional applications of chiral mechanical metamaterials: A review," *Materials & design*, vol. 180, p. 107950, 2019.
- [65] P. Chebychev, "Théorie des mécanismes connus sous le nom de parallélogrammes, 2ème partie," *Mémoires présentés à l'Académie impériale des sciences de Saint-Petersbourg par divers savants*, 1869.
- [66] Q. Li, D. Yang, C. Ren, and X. Mao, "A systematic group of multidirectional buckling-based negative stiffness metamaterials," *International Journal of Mechanical Sciences*, vol. 232, p. 107611, 2022.

-
- [67] H. M. Kolken and A. Zadpoor, "Auxetic mechanical metamaterials," *RSC advances*, vol. 7, no. 9, pp. 5111–5129, 2017.
- [68] N. Novak, M. Vesenjajk, and Z. Ren, "Auxetic cellular materials-a review," *Strojniški vestnik-Journal of Mechanical Engineering*, vol. 62, no. 9, pp. 485–493, 2016.
- [69] W. Yang, Z.-M. Li, W. Shi, B.-H. Xie, and M.-B. Yang, "Review on auxetic materials," *Journal of materials science*, vol. 39, no. 10, pp. 3269–3279, 2004.
- [70] C. P. de Jonge, H. M. Kolken, and A. A. Zadpoor, "Non-auxetic mechanical metamaterials," *Materials*, vol. 12, no. 4, p. 635, 2019.
- [71] K. E. Evans, M. Nkansah, I. Hutchinson, and S. Rogers, "Molecular network design," *Nature*, vol. 353, no. 6340, pp. 124–124, 1991.

Analyzing out-of-plane deformations caused by varying Poisson ratio distributions in a metamaterial

Abstract

Auxetic metamaterials offer various novel abilities, one of the abilities is to deform into a dome-shape under out-of-plane deformation. Contrary to a material with a positive Poisson's ratio, which deforms into a saddle-shape. A dome-shape is named synclastic deformation and a saddle-shape is named anticlastic deformation. Under out-of-plane deformation, the magnitude and sign of the Poisson's ratio influence the curvature of the material, and hence the final shape. Starting from a flat plane, manipulation of the Poisson's ratio can create various unusual shapes, such as an egg or a wave-shape. A desired shape might require a uniform Poisson's ratio or a varying Poisson's ratio distribution. Most of the current estimations on the relation between an auxetic material and the deformation shape are performed experimentally. This paper presents an analytical approach which shows the influence of a varying Poisson's ratio on the out-of-plane deformation of a material under pure bending conditions. Four Poisson's ratio distributions are applied which follow the formulas: S-curve, parabolic and cosine in one and two directions. The same model is build in the FEM software COMSOL which serves as the reference model. Comparison of the COMSOL model shows a Mean Absolute Percentage Error between 0.30% and 11.93% for the analytical model. Remarkably, the accuracy of the analytical model is high if a Poisson's ratio distribution varies in one direction, resulting in a Mean Absolute Percentage Error lower than one percent point. A limitation of the analytical model is that the Mean Absolute Percentage Error (MAPE) increases to 0.69% till 11.93% when the Poisson's ratio varies in two directions. The presented analytical approach provides a first step in determining a varying Poisson's ratio distribution that can deform into any desired shape. The resulting shapes are synclastic and combinations of synclastic and anticlastic.

1. Introduction

All materials that we see around us, such as the piece of paper one might read this article on, have their own unique

material properties. These material properties describe the behavior of the material under certain conditions. Recently, researchers have been trying to extend the limits of mechanical materials. The newly researched materials that exhibit unusual mechanical properties are called mechanical metamaterials (1). A mechanical metamaterial might obtain negative stiffness, a negative or zero Poisson's ratio or negative compressibility by altering the internal geometrical structure (2).

Most research on the Poisson's ratio property focuses on presenting internal structures that create a negative Poisson's ratio (3; 4). A negative Poisson's ratio also offers novel abilities which a positive Poisson's ratio could not. One of the novel abilities is the capacity for synclastic deformation under out-of-plane bending (5). A synclastic deformation is when an object deforms to the shape of a dome. There are two other types of deformations, all of which are visualized in Figure 3.1 with the corresponding Poisson's ratio. The second is the anticlastic deformation, which is a saddle shape and results from a positive Poisson's ratio. The third is the monoclastic which is a cylinder shape and is caused by a zero Poisson's ratio.

The synclastic ability is, however, not often studied yet. An application possibility is reviewed of replacing the current material in a synclastic part with an auxetic metamaterial. The auxetic metamaterial is deemed a good replacement for the current material due to its ability to deform synclastic and a better indentation resistance, which is another advantage of an auxetic metamaterial. Yet, the metamaterial is pre-shaped to fit into the application (6). A synclastic shape can also be achieved by applying out-of-plane deformation on a flat plane. Callens and Zadpoor have reviewed that various origami and kirigami tessellations are able to achieve a synclastic deformation. Specific tessellations also show a combination of a synclastic and anticlastic surface (7). For example, Dudte et al have shown that by varying the geometrical parameters of a Miura-ori fold, various synclastic shapes can be realized (8).

Besides origami and kirigami tessellations, cellular structures are also able to a deform synclastically under

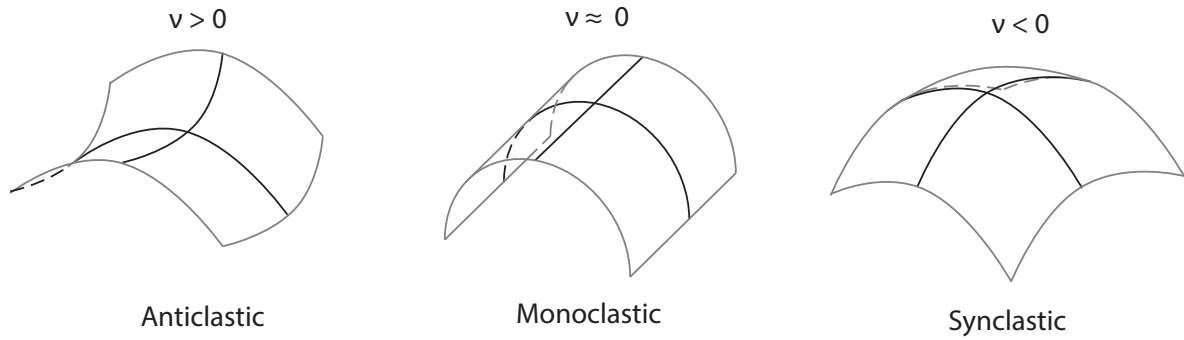


Figure 3.1: Models depicting anticlastic, monoclastic and synclastic deformation and their corresponding Poisson's ratio value.

out-of-plane bending while starting from a flat state. For example, Mirzaali et al have shown that a synclastic surface can be achieved for a re-entrant honeycomb tessellation. Furthermore, they derived an out-of-plane deformation formula with experimentally derived parameters which assist in predicting the final shape of the material (9). A more direct approach is possible as well, for instance by using the knowledge that a torus shape needs a negative, zero and a positive Poisson's ratio. Interpolation of cellular patterns that have the required Poisson's ratio of $\nu = -1$, $\nu = 0$ and $\nu = 1$ creates a torus (10). Both these studies have shown that a honeycomb tessellation can be deformed into a gradient to achieve various shapes, may it be a synclastic shape or a combination of synclastic and anticlastic.

To achieve more detail in the Poisson's ratio gradient, a computational analysis can be applied which can aid in computing the deflection of the material under complex loading conditions. The combination of the direct approach and a FEM approach resulted in the fabrication of a seating cushion, hence a surface that flows from a synclastic shape to an anticlastic shape to again a synclastic shape(11). A next step in computational analysis would be to introduce an optimization method to compute the internal structure of the material (12).

From the reviewed literature it is clear that an auxetic material can deform in a synclastic shape. However, an exploration into the analytical relation of the Poisson's ratio and out-of-plane deformation is missing. An analytical base will strengthen the understanding how a desired shape can be achieved. Moreover, metamaterials allow for a varying distribution of the cellular structure and thus a variation in Poisson's ratio. A material with a varying Poisson's ratio distribution will open a new range of shape forming possibilities.

This study aims to determine an analytical approach for the out-of-plane deformation of a plate with a varying Poisson's ratio distribution under pure bending conditions. The analytical model will provide a clear understanding of the Poisson's ratio relation and the out-of-plane deformation. It will create a base from which, in future research, more complex shape may be obtained. Furthermore, the proposed analytical model may simplify future optimization analyses because the formulas are straightforward.

Four variants in Poisson's ratio distributions are applied in the material, two distributions vary in one direction and the other two distributions vary in two directions. The plate is analyzed under pure bending conditions. The results of the analytical approach are compared and validated with the outcome of a simulation in the FEM software COMSOL.

First, relevant theoretical definitions are introduced (section 2). Next, the research method is detailed (section 3), followed by obtained results (section 4.). After follows discussion of the results (section 5) before the study's conclusion (section 6).

2. Background

The focus of this paper is on the out-of-plane deformation of a geometry as a result of the auxetic property. The relation of bending curvature and the Poisson's ratio is described in subsection 2.1. Next, in subsection 2.2 the equations are outlined that belong to pure bending conditions. Pure bending is elaborated with numerical integration which is detailed in subsection 2.3.

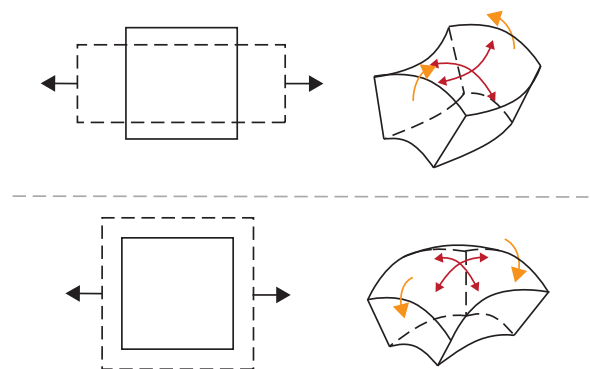


Figure 3.2: Top: anticlastic deformation given a positive Poisson's ratio. Bottom: synclastic deformation given a negative Poisson's ratio.

2.1. Auxetic and synclastic deformation

The Poisson's ratio is a mechanical material property which defines a ratio between transverse deformation(ϵ_x) and

axial (ϵ_y). Elongating deformations are positive and compressive deformations are negative. Hence the definition has a minus sign so that conventional materials have a positive Poisson's ratio for clear interpretation.

$$\nu = -\frac{\epsilon_x}{\epsilon_y} \quad (3.1)$$

Thus, when a 'normal' material is compressed, it will elongate along the perpendicular direction. When a part is bended, one side will compress while the other side will elongate. This causes the material to create a saddle-shape under out-of-plane bending (Figure 3.2, top) (13).

Materials that are auxetic, deform differently from the 'normal' materials. When an auxetic material is compressed, it will compress along the perpendicular direction as well. The difference in the sign of the Poisson's ratio causes the material to deform differently when out-of-plane bending is applied. Under out-of-plane deformation, an auxetic material will create a dome shape instead of a saddle-shape (Figure 3.2, bottom) (5). In this way, the curvature of an objects depends on the Poisson's ratio of the material.

2.2. Pure bending

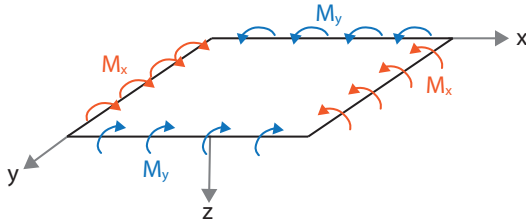


Figure 3.3: Pure bending conditions for a plate in a 3D-coordinate system (13).

Pure bending is a loading condition in which the model is subjected to a constant bending moment (Figure 3.3). Due to the constant bending moment, the axial and shear forces are equal to zero. The relation of the deformation of the geometry and the applied moment is defined according to the book *Theory of plates and shells* by S. Timoshenko (13):

$$\begin{bmatrix} M_x \\ M_y \\ M_{xy} \end{bmatrix} = - \begin{bmatrix} D & \nu D & 0 \\ \nu D & D & 0 \\ 0 & 0 & D(1-\nu) \end{bmatrix} \begin{bmatrix} \kappa_x \\ \kappa_y \\ \kappa_{xy} \end{bmatrix} \quad (3.2)$$

M is the applied moment, ν the Poisson's ratio and κ is the curvature. Lastly, the flexural rigidity of the plate, D , is defined as:

$$D = \frac{Eh^3}{12(1-\nu^2)} \quad (3.3)$$

E is the Young's modulus of the material and h is the height of the geometry.

Rewriting Equation 3.2 and substituting Equation 3.3, we obtain the equations that describe the curvature in x - and y -direction.

$$\begin{aligned} k_x &= -\frac{M_x - \nu M_y}{D(1-\nu^2)} = -12 \frac{M_x - \nu M_y}{Eh^3} \\ k_y &= -\frac{M_y - \nu M_x}{D(1-\nu^2)} = -12 \frac{M_y - \nu M_x}{Eh^3} \end{aligned} \quad (3.4)$$

2.3. Numerical integration

The out-of-plane displacement (w) can be determined by the equation:

$$w = -\frac{M_x - \nu M_y}{2D(1-\nu^2)} x^2 - \frac{M_y - \nu M_x}{2D(1-\nu^2)} y^2 + C_1 x + C_2 y + C_3 \quad (3.5)$$

in which C_1 , C_2 and C_3 are determined by the boundary conditions. However, Equation 3.5 does not enable a varying Poisson's ratio. Hence, the out-of-plane displacement is determined through numerical integration which necessitates the curvature and the slope of the whole plane. The curvature is the second derivative of the out-of-plane displacement, $\kappa_x = \frac{d^2 w}{dx^2}$. Using Euler's numerical integration with a step-size s_x and s_y , the slope ($\frac{dw}{dx}$) of out-of-plane displacement is determined (14).

$$\begin{aligned} \frac{dw}{dx}_{i+1} &= \frac{dw}{dx}_i + \frac{d^2 w}{dx^2}_i \cdot s_x \\ \frac{dw}{dy}_{i+1} &= \frac{dw}{dy}_i + \frac{d^2 w}{dy^2}_i \cdot s_y \end{aligned} \quad (3.6)$$

Displacement of the entire field is then determined by incorporating slope and curvature in the x - and y -directions (Figure 3.4) (13).

$$\begin{aligned} w_{i+1,j+1} &= w_{i,j} + \frac{dw}{dx}_{i+1,j} s_x + \frac{dw}{dy}_{i,j+1} s_y \\ &+ \frac{d^2 w}{dx^2}_{i+1,j} \frac{s_x^2}{2} + \frac{d^2 w}{dy^2}_{i,j+1} \frac{s_y^2}{2} \end{aligned} \quad (3.7)$$

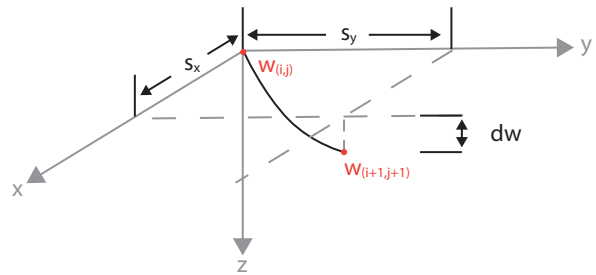


Figure 3.4: Schematic display of the path from the initial displacement node $w_{(i,j)}$ to the next displacement node $w_{(i+1,j+1)}$ at a distance s_x and s_y .

3. Method

The deformation of a plate is analyzed under pure bending conditions and determined in MATLAB. The outcome of MATLAB is validated with the FEM software COMSOL. The geometrical and material properties of the model is described in subsection 3.1. The constraints put upon the model are presented in subsection 3.1 as well. Next, the deformation of the model will be determined using a pure bending approach in combination with a numerical integration approach, respectively in subsection 3.2 and subsection 3.3. The details of the COMSOL setup can be found

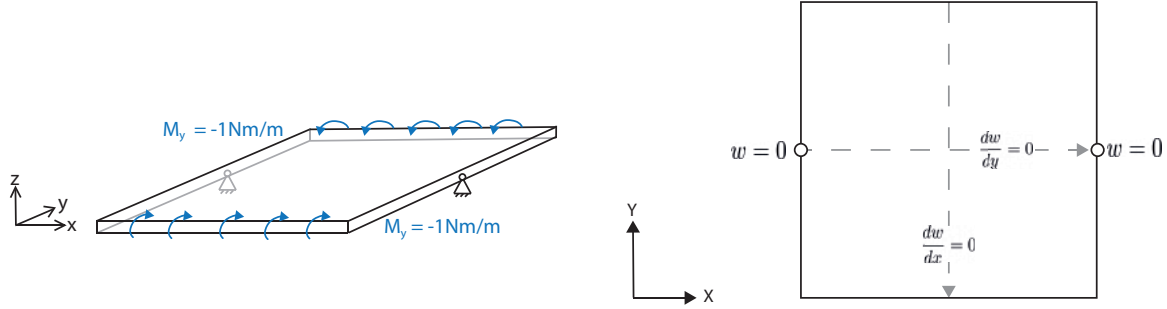


Figure 3.5: An overview of the constraints put on the plate. Left: schematic view of the plate and the two rotational joints. The applied bending moment marked with blue arrows. Right: location marked where the deformation is equal to zero and the slope lines that are equal to zero satisfying double-symmetry conditions.

in subsection 3.4. Four variants of Poisson's ratio distribution are applied in the analytical model and in the COMSOL setup. The four variants are laid out in subsection 3.5.

3.1. Simulation model

For the scope of this study, a square plate is chosen as the test geometry, as it suffices for implementation of the pure bending conditions. The plate dimensions and material properties are listed in Table 3.1. The listed material properties are taken from silicone rubber (15). Plate theory is used to determine the deformation.

Width, length (l)	0.2 [m]
Height (h)	10^{-3} [m]
Young's Modulus (E)	$25 \cdot 10^6$ [Pa]
Density (ρ)	1500 [kg/m ³]

Table 3.1: Material properties of silicone rubber and geometry dimensions.

Plate constraints are chosen such that the plate has as much freedom as possible in the z-direction to ensure that the deformation is a result of the material properties. The plate is constrained at two opposing ends with two rotational joints.

3.2. Pure bending

To understand the influence of the Poisson's ratio, a simple loading condition is chosen. Pure bending is selected as it eliminates the contributions of the shear and axial forces and thus simplifying the deformation equations (to Equation 3.2). The plate is subjected to a bending moment of $M_y = -1 \text{ Nm/m}$ and $M_x = 0 \text{ Nm/m}$. Applying M_y and M_x would cause the deflection of the plate to be imposed by the direction of the applied loading condition and not the material properties. Whereas if $M_x = 0 \text{ Nm/m}$, the deflection of the plate is a result of the material properties.

The combination of the model geometry, pure bending and two rotational joints ensures double-symmetry in the model. A double-symmetric model provides the boundary conditions $\frac{dw}{dx} = 0$ along $y = 0 \text{ m}$ and $\frac{dw}{dy} = 0$ along $x = 0 \text{ m}$. These boundary conditions make the deflection computation more straight-forward. An overview

of the aforementioned constraints and boundary conditions is provided in Figure 3.5.

3.3. Numerical integration

To accommodate a varying Poisson's ratio distribution, numerical integration is applied to Equation 3.2 to obtain the out-of-plane deformation of the plate. Using numerical integration allows for a different value for the Poisson's ratio at every integration step. The numerical integration is done with the Euler-method with a step-size $s_x = s_y = 10^{-3} \text{ [m]}$ (14). A small step-size allows for a linear approach to determine the deformation. Linearity is preferable as it has a lower computation time compared to a non-linear model and results in less complicated equations. It is assumed that the end of the numerical integration node deforms straight down and that thus the x- and y-coordinates of that node remain the same after deformation (see Figure 3.7).

As the model is double-symmetric, it suffices to compute the deformation of one quarter of the square plate. The full deformation is then derived by mirroring that one quarter over the center x- and y-axes. The order in which the deformation is built up is depicted in Figure 3.6. The corresponding MATLAB-code can be found in Appendix C

Out-of-plane deformation for one quarter is established following Equation 3.7. A visualization of the integration steps taken can be seen in Figure 3.6. Before computing Equation 3.7, the displacement of a single horizontal line is determined. The numerical integration starts at the location of the left rotational joint because it is known that the displacement at that node is equal to zero. From that point, the numerical integration direction follows along the x-direction to the center to obtain the horizontal deformation line. The next step, starting from the nodes determined at the horizontal line, is numerical integration along the y-direction to construct the deformation of the full quarter. The deflection is obtained using Equation 3.7. Depending in which direction the integrating is taken, determines whether the step-size s_x or s_y is equal to zero.

3.4. COMSOL setup

The COMSOL setup tries to follow the prescribed model from the previous sections as closely as possible. Two com-

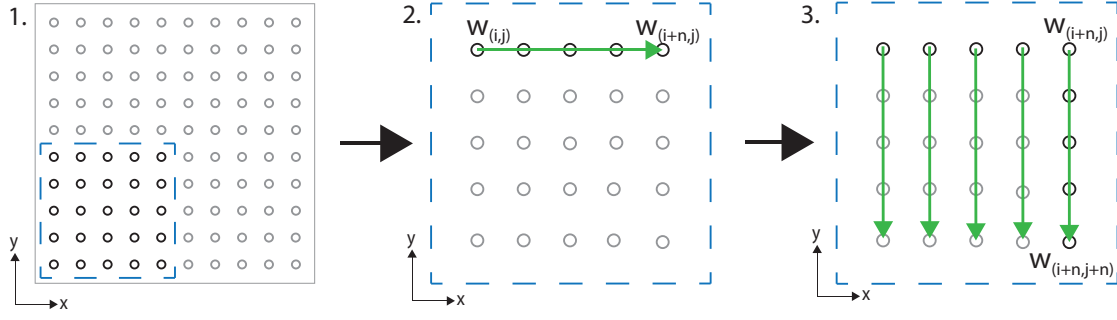


Figure 3.6: The numerical integration sequence to obtain the displacement of one quarter of the plate.

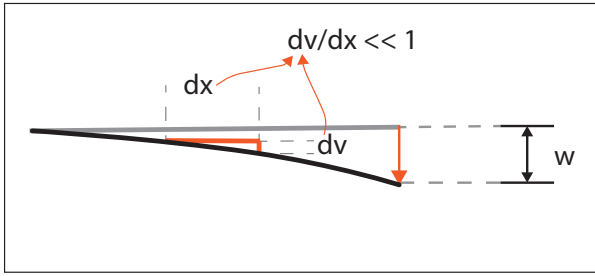


Figure 3.7: Linear displacement criteria for bending of a beam-segment.

ponents are different between the analytical model and the COMSOL setup. The first component concerns the part that is attached to the rotational joint. In the model this part is simulated as a node which make the model under-constraint because a rotation about the y -axis is possible. To eliminate the rotation, a small line of $d = 2 \cdot 10^{-3}$ m is modeled in the COMSOL setup at the node location.

The second part is the element size in the mesh. In the analytical model the mesh consists of squares with sides of $l = 10^{-3}$ m. The mesh in the COMSOL setup is build up with triangles using the normal-setting in the COMSOL software. Initial analysis on the impact of the element-size (coarse, normal and fine-settings) of the mesh on the output concluded that the effect of the element-size were negligible. A square mesh would extend the computation time and thus the element-size remained triangular. The difference in mesh size leads to the requirement of the output data from the COMSOL model to be post-processed in MATLAB (see Appendix B). The post-processing consist of interpolating the data with the MATLAB-function `griddata` to achieve a similar size dataset.

3.5. Poisson's ratio

Four variants of Poisson's ratio distributions are embedded in the material properties of the plate. Two distributions vary in x -direction and the other two distributions vary in both the x - and y -direction. All are depicted in Figure 3.8.

For each variant of Poisson's ratio distribution, three Poisson's ratio range-sets are analyzed. Every set has a $|\Delta v| \approx 0.4$:

- Set 1: the distribution is in the positive Poisson's ratio domain. The distributions has a minimum of $v \approx 0$ and a maximum of $v \approx 0.4$.
- Set 2: the distribution is in the negative as well as in the positive domain. The minimum value is $v \approx -0.2$ and the maximum values is $v \approx 0.2$.
- Set 3: the distribution is entirely in the negative domain with a minimum value of $v \approx -0.4$ and a maximum value of $v \approx 0$.

S-curve

The first variant is a S-curve distribution and varies in the x -direction. The distribution is described by the equation:

$$v(x, y) = \begin{cases} \frac{2}{5} \frac{1}{(1+e^{-k(x+0.05)})^a} + b & \text{if } x \leq 0 \\ \frac{2}{5} \frac{1}{(1+e^{-k(x-0.05)})^a} + b & \text{if } x > 0 \end{cases} \quad (3.8)$$

$$a = 2$$

$$k = 200$$

$$b = [0 \quad -0.2 \quad -0.4]$$

The multiplication factor $\frac{2}{5}$ is applied to ensure that the v -range is equal to 0.4. Next, the parameter ± 0.05 in the exponent is to set the location of the shift in Poisson's ratio value at a quarter of the width. Furthermore, the parameters a and k are tuned for the desired s-curve shape. Finally, parameter b is set to achieve the three Poisson ratio range-sets.

Cosine one directional

The second Poisson's ratio distribution that varies in the x -direction follows the cosine equation:

$$v(x, y) = \frac{1}{5} \cos\left(\frac{2\pi}{0.1} x\right) - b \quad (3.9)$$

$$b = [-0.2 \quad 0 \quad 0.2]$$

The $\cos(x)$ equation has a range from -1 till 1 , hence the reason for the multiplication factor to be $\frac{1}{5}$ to achieve a range of $v = 0.4$. Next, the period of the cosine should be 0.1 leading to the parameter $\frac{2\pi}{0.1}$. Lastly, the parameter b is set to attain the three Poisson ratio range-sets.

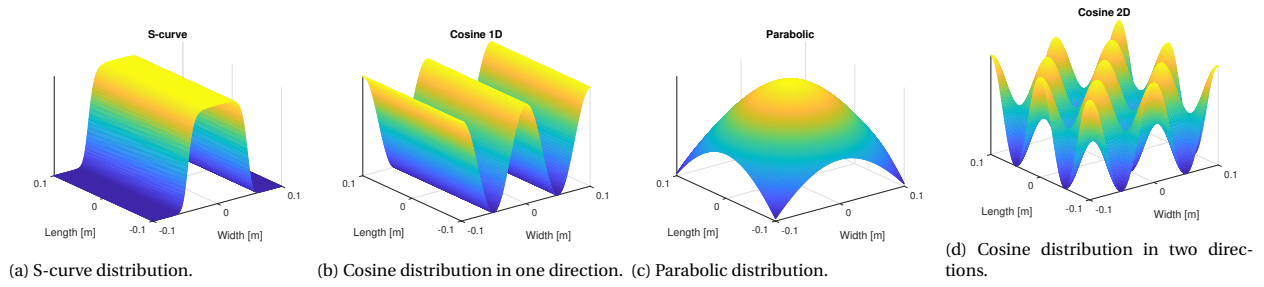


Figure 3.8: The four Poisson's ratio distributions.

Parabolic

The parabolic Poisson's ratio distribution is a gradual distribution in two directions:

$$v(x, y) = -C \sqrt{D + \frac{x^2}{A^2} + \frac{y^2}{B^2}} - b \quad (3.10)$$

$$A = 0.1$$

$$B = 0.1$$

$$C = \sqrt{\frac{v_c^2}{D}}$$

$$v_c = 0.4$$

$$D = 1$$

$$b = [0.4 \quad 0.6 \quad 0.9]$$

The parameters A and B are chosen such that the Poisson's ratio variant fits within the boundaries of the plate. C depends on v_c and D . v_c is chosen such that the variant has approximately the desired height and D determines whether the variant is a dome or a valley shape. Finally, b is set such that the Poisson's ratio range-sets can be attained.

Cosine two directional

The final Poisson's ratio distribution is the cosine equation in two directions:

$$v(x, y) = \frac{1}{5} \cos\left(\frac{2\pi}{0.1}x\right) \cdot \cos\left(\frac{2\pi}{0.1}y\right) - b \quad (3.11)$$

$$b = [-0.2 \quad 0 \quad 0.2]$$

The parameters of the last Poisson's ratio variant are chosen in the same manner as for the cos 1D variant.

3.6. Error measurement

To measure the accuracy of the analytical model, two error measurement types are computed. The first is the Mean Absolute Error (MAE) and the second is the Mean Absolute Percentage Error (MAPE).

Mean Absolute Error

The MAE is an error measurement that computes the absolute difference between the COMSOL value and the analytically derived value at every node. The equation is formulated as:

$$\text{MAE}(i, j) = |Z(i, j) - w(i, j)| \quad (3.12)$$

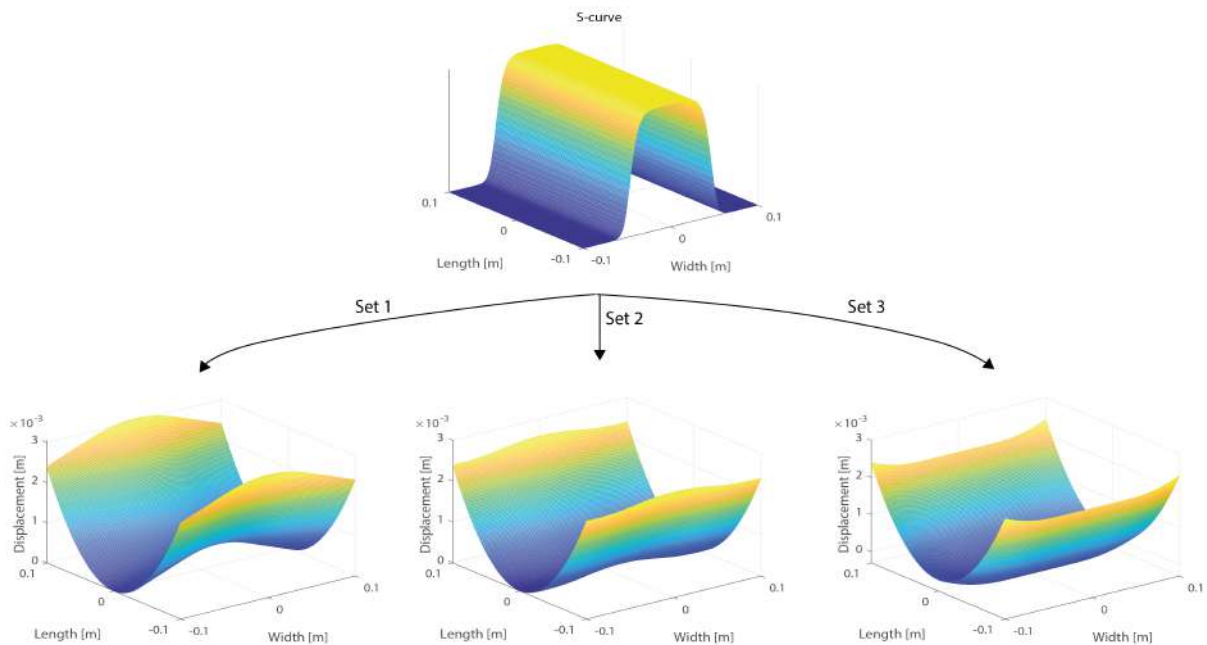


Figure 3.9: The three displacement fields resulting from pure bending of a plate containing S-curve Poisson's ratio variation.

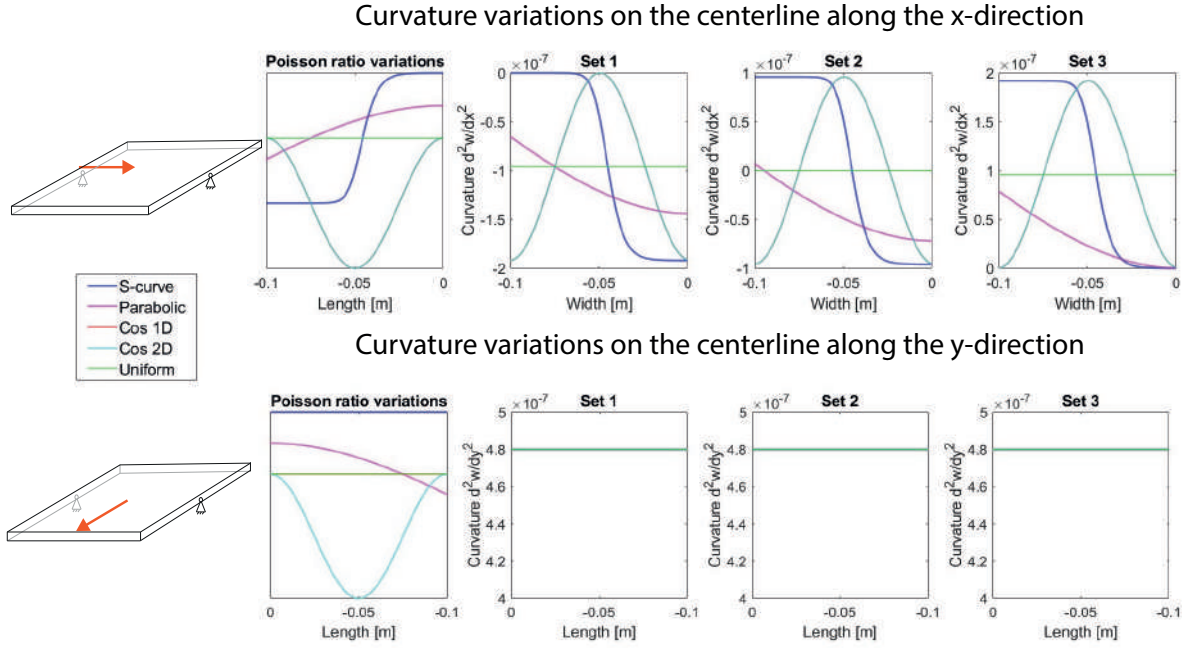


Figure 3.10: Curvature propagation of each Poisson's ratio variant and a uniform Poisson's ratio along the x - and y -direction. The top half depicts the curvature propagation in the x -direction and the bottom half in the y -direction. Graph on the left depicts the Poisson's ratio curve, the next three graphs depict the curvature per Poisson's ratio range-set.

Z is the deflection of the COMSOL model and w is the analytically derived deflection.

Mean Absolute Percentage Error

The second error measurement is MAPE which expressed the error between the COMSOL output and the analytical model in a percentage value.

$$\begin{aligned}
 e(i, j) &= |Z(i, j) - w(i, j)| \\
 p(i, j) &= \frac{e(i, j)}{|Z(i, j)|} \cdot 100 \\
 \text{MAPE} &= \frac{\sum p(i, j)}{N}
 \end{aligned} \quad (3.13)$$

The deflection derived with the analytical approach is represented with $w(i, j)$, the deflection derived by COMSOL is represented with $Z(i, j)$ and N is the number of values.

4. Results

The results are sectioned to first consider the effect of a varying Poisson's ratio on the behavior of the model. Next, the limitations of the analytical model are observed. Lastly, the shape-following capabilities are displayed.

4.1. Effect of a varying Poisson's ratio distribution

An initial view is provided in Figure 3.9 that displays the effect of the S-curve Poisson's ratio variation on the out-of-plane deformation of a plate. The three resulting deflections of each Poisson's ratio range-set are visualized to distinguish the effect of the sign of the Poisson's ratio. The deflection of Poisson's ratio range-set 1, all Poisson's ratio

values are positive, is anticlastic. The second Poisson's ratio range-set, which has a Poisson's ratio going from negative to positive values, has anticlastic and synclastic deformation. Lastly, the third Poisson's ratio range-set, all Poisson's ratio values are negative, depicts a synclastic deformation. An overview of all twelve displacement simulations is provided in Appendix A.

To further understand the relation between the Poisson's ratio and the out-of-plane deformation, the curvature propagation of the model is analyzed. A uniform Poisson's ratio is applied to the analytical model as well to properly identify the effect of a varying Poisson's ratio. The uniform Poisson's ratio will create a uniform curvature in a pure bending loading condition. Hence, when the curvature deviates, the effect varying Poisson's ratio will be clear. The curvature of the model is displayed in Figure 3.10. Lastly, because the model is double-symmetric, it suffices to analyze the bottom-left quarter of the model, indicated with blue dotted lines in Figure 3.6.1.

Figure 3.10 displays the curvature trajectory of the analytical model for every set along the centerlines in the x - and y -direction (visualized with red arrows in Figure 3.10). The curvature is analyzed for the centerline in the x -direction because this line is the second step in the numerical integration. For curvature analysis in the y -direction, any line would have sufficed. The depicted line is chosen arbitrarily because the third step in the numerical integration method shows that the approach for each y -line is the same. The top half graphs show, from left to right, the Poisson's ratio variations, the curvature propagation along the centerline in the x -direction from $x = -0.1m$ till $x = 0m$ for set 1, set 2 and set 3. The two

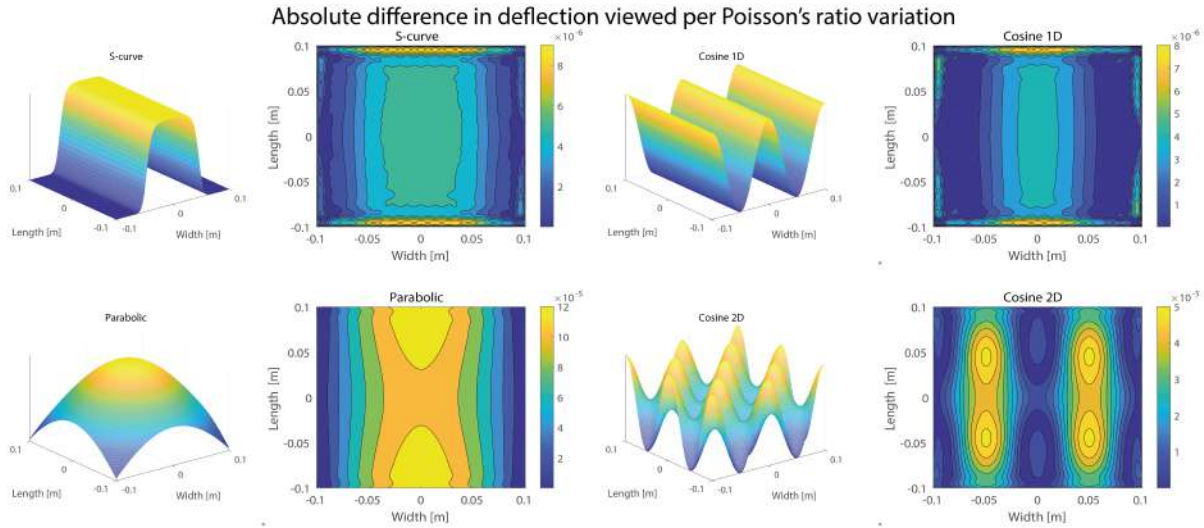


Figure 3.11: The averaged propagation of the MAE between the analytical model and COMSOL. The MAE is displayed for each Poisson's ratio variant and averaged over the Poisson's ratio range-sets.

Poisson's ratio variants cosine 1D and cosine 2D overlap. The overlap creates the darker green shade which is seen in all three of the top curvature propagation graphs. Furthermore, in the three top graphs one can see that the curvature varies greatly in the x -direction. The minimum and maximum value for the curvature is the same every Poisson's ratio variation except for the parabolic distribution.

The bottom half of Figure 3.10 depicts, from left to right, the same types of graphs as the top half. The curvature propagation is depicted along the centerline in the y -direction from $y = 0m$ till $y = -0.1m$ and is again for clarification visualized with a red arrow. In the Poisson's ratio graph, the uniform Poisson's ratio and the cosine 1D overlap and create a olive-tone green line. The three bottom graphs show that the curvature remains constant along the y -direction.

4.2. Comparison analytical model and COMSOL model

The analytical model with the pure bending approach is compared and validated with the FEM software COMSOL. The initial validation of the analytical model for a uniform Poisson's ratio ranging from $\nu = [-0.8 \ -0.6 \ -0.4 \ -0.2 \ 0 \ 0.2 \ 0.4 \ 0.6 \ 0.8]$ can be found in Appendix D. To determine the accuracy of the analytical mode with a varying Poisson's ratio, the Mean Absolute Percentage Error (MAPE) value is computed. The MAPE is determined for every Poisson's ratio variant and for each Poisson's ratio range-set, of which the resulting values can be found in Table 3.2.

As a result of the COMSOL output-data being processed in MATLAB, the nodes align with the rotational joints are not zero. This results in peaks found in the p -matrix. To resolve this, the MATLAB function `rmoutliers` is used which detects and removes outliers in the p -matrix from Equation 3.13. The outliers are removed by using the default method of MATLAB, namely the `median`-method.

In general, the MAPE is higher when a varying Poisson's ratio is implemented. Noteworthy is the difference in accuracy between the four Poisson's ratio variations. The MAPE is below one percent for the S-curve and cosine 1D variation but higher for the parabolic and the cosine 2D variation. The MAPE stands out the most for the parabolic variation as the values are the highest.

	S-curve	Cosine 1D	Parabolic	Cosine 2D
Set 1	0.30%	0.23%	5.14%	1.80%
Set 2	0.42%	0.35%	7.04%	2.41%
Set 3	0.69%	0.36%	11.93%	2.30%

Table 3.2: The MAPE value for every Poisson's ratio variant and set range.

A detailed outline of the Mean Absolute Error (MAE) between the analytical model and COMSOL throughout the plane is depicted in Figure 3.11. Per Poisson's ratio variant, the MAE is computed for each Poisson's ratio range-set. The resulting MAE from the three sets are averaged:

$$MAE_{all}(i, j) = \frac{\sum_k^3 MAE_k(i, j)}{3} \quad (3.14)$$

In Figure 3.11, the colorbar has the same color range for each graph, however, the range in magnitude varies per graph. The region in which the absolute difference is the largest is thus depicted in yellow. The propagation of the MAE is similar for the S-curve and the cosine 1D variations. A bigger difference is seen for the parabolic and cosine 2D variations.

4.3. Shape following

Lastly, the shape generation by applying a varying Poisson's ratio distribution is studied. The cosine 1D Poisson's ratio variation is chosen to exemplify how a varying Poisson's ratio distribution can display various shapes. In Figure 3.12, one can see how a part of the cosine 1D Poisson's ratio variant follows the synclastic shape of an Easter-egg.

Another part shows the synclastic and anticlastic combination of a flower vase.

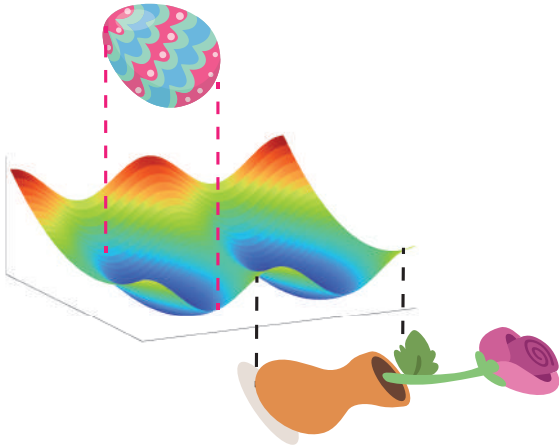


Figure 3.12: Part of the cosine 1D Poisson's ratio variation in which the shape of an Easter-egg and flower vase can be found (16; 17).

5. Discussion

This study aims to determine the out-of-plane deformation of a material with a varying Poisson's ratio distribution through using an analytical approach. A clear understanding of the relation between the deformation shape and the material's Poisson's ratio can strengthen the understanding of how a desired shape can be achieved. Four Poisson's ratio variants are applied to analyze the difference in output-response. The analytical model is compared with the FEM software COMSOL which in turn will show the limitations of the analytical model.

In Figure 3.10 it can be seen that the Poisson's ratio variant has an effect of the curvature along the x -direction, but does not have an effect on the curvature along the y -direction. The reason for this can be understood by substituting the applied bending moments in Equation 3.4. The resulting formula for the curvature in the x -direction remains depended on the Poisson's ratio and the formula for the curvature in the y -direction does not depend on the Poisson's ratio anymore.

$$\begin{aligned} k_x &= -12 \frac{\nu}{Eh^3} \\ k_y &= 12 \frac{1}{Eh^3} \end{aligned} \quad (3.15)$$

Under the applied conditions, the curvatures k_y always remains positive and constant. Until a bending moment M_x is applied, the curvature in the y -direction will not vary. If a moment M_y and M_x are applied, more deformation shapes can be achieved. However, for the purpose of this study, one bending moment M_y was adequate because the purpose of the study was to highlight the effect of the Poisson's ratio.

The trajectories of the curvatures k_x have the same maximum and minimum point for the Poisson's ratio variants S-curve, cosine 1D and cosine 2D. The parabolic variant has a different minimum and maximum because along

the x -centerline, the Poisson's ratio range is smaller than of the other three variants.

The accuracy of the model is high when a uniform Poisson's ratio is applied. When a varying Poisson's ratio distribution is applied to the model, the accuracy of the analytical model decreases. In Appendix D it was seen the

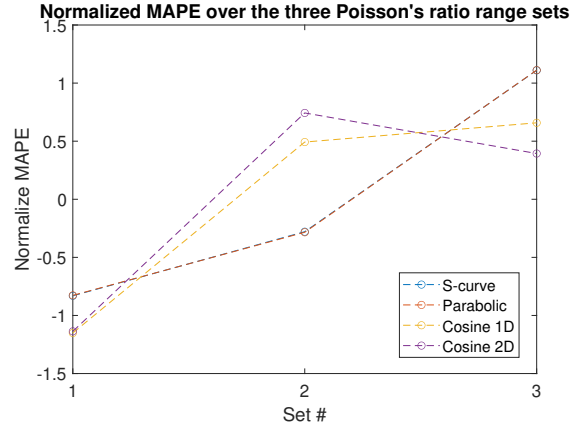


Figure 3.13: The trajectory of the normalized MAPE for each Poisson's ratio variant.

Mean Absolute Percentage Error (MAPE) did not go beyond 0.12% when a uniform Poisson's ratio was applied, whereas the minimum MAPE with a varying Poisson's ratio distribution is 0.23% and increases to 11.93%. The MAPE values are satisfactory which allows for further elaboration on the analytical model and possible usage in an optimization analysis. A distinction in accuracy can be made between the Poisson's ratio variants which vary in one direction

(S-curve and cosine 1D), and the two variants that vary in two directions (parabolic and cosine 2D). It seems that when the Poisson's ratio distribution contains more variation, the accuracy decreases. The decrease in accuracy may be due to the increase in Poisson's ratio variation. More Poisson's ratio variation causes larger deviations in the governing equations which in turn makes the equations more prone to truncation errors. A small trend is found in the MAPE propagation for the Poisson's ratio variants in Figure 3.13. The trajectory for the S-curve and the parabolic variant overlap exactly, and the trajectory for the cosine 1D and cosine 2D overlap almost. The deviation in trajectory could be attributed to the cosine variants decreasing and increasing in Poisson's ratio whereas the S-curve and parabolic variants only increase in the same period.

Two things can be considered to increase the accuracy of the analytical model which will improve the model. The first lies in resolving the global truncation error, a cumulative error caused by multiple integration steps. As stated in subsection 3.4, the nodes that should be zero are not. The initial offset is around $|e_{\text{offset}}| = 2.2 \cdot 10^{-7}$ for every data-set. The resulting truncation error can be minimized by using a more refined numerical integration method, such as the Heun or Runge-Kutte 4 method. Both methods will increase the computation time of the model but

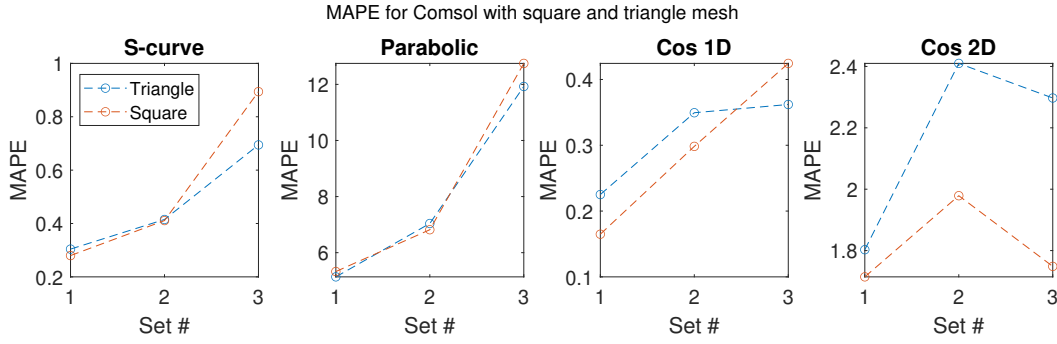


Figure 3.14: The MAPE for a square and triangular mesh. Viewed per Poisson's ratio variation and range-set.

increase the accuracy. To in turn decrease the computation time, the step-size might be increased.

The second aspect to be considered is the element size used in the mesh for the COMSOL model. A mesh element in similar size and shape is applied in the COMSOL-model. The resulting MAPE are visualized in Figure 3.14 next to the MAPE's listed in Table 3.2. Applying a square mesh in COMSOL results in a similar output compared to the model with the triangle mesh for the S-curve and parabolic variant. Interestingly, for the cosine 2D variant, the square mesh perform significantly better. This result suggest that it is worth looking into if another mesh for both models could increase the accuracy. It must be taken into account that applying the square mesh requires more computation time because the mesh consisted of more elements. Perhaps a mesh with square elements but a larger size will result in a higher accuracy.

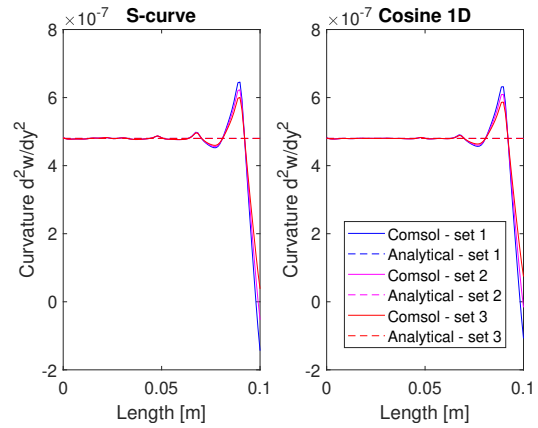


Figure 3.15: The curvature $\frac{d^2w}{dy^2}$ propagation for the analytical model and the COMSOL model along an arbitrary line in the y -direction.

Figure 3.11 provides more detail on the propagation of the Mean Absolute Error (MAE) for each Poisson's ratio variant. The two Poisson's ratio variants which vary in one direction show similar propagation trajectories and magnitude. The maximum MAE's are located in the center of the y -edges (around $x = 0m$ $y = \pm 0.1m$). It is expected that the maximum MAE is located along the y -line with $x = 0m$ as a result of the truncation error. Because the curvature k_y is constant, it is not expected that the truncation error becomes much larger. However, the MAE increases notably towards the edge. A look into the curvature propagation along an arbitrary line in the y -direction reveals that the curvature does not remain constant in the COMSOL model (seen in Figure 3.15). The peaks in the curvature may be due to an error of FEM computation in COMSOL. For FEA, proper boundary conditions need to be set in place. In this study, the edges of the analyzed geometry are free to move in which ever direction. The error in the FEM computation may be due to the boundary conditions being underdefined and hence complicating the governing FEM-equations along the edges (18). The error might be mitigated by applying a finer mesh at the specified edge-nodes.

The MAE propagation for the parabolic and cosine 2D variant seem to follow the shape of the corresponding Poisson's ratio variant. The MAE propagation for both can be further explained when we take a look into the deflection of the centerline along the x -direction. An interest-

ing aspect is that the deflection of the parabolic variant only diverges whilst the deflection of the cosine 2D variant diverges and converges (see Figure 3.16). The diverging and converging behavior is in line with the Poisson's ratio propagation and correspondingly also in line with the MAE propagation. The converging behavior of the cosine 2D variant is probably also the cause for the accuracy of the cosine 2D variant being higher than the parabolic variant.

Lastly, the shape forming capabilities are discussed. From Figure 3.12 it can be seen that the synclastic shape of an egg can be achieved. Another shape which is double-curved, such as a flower vase, can also be achieved by varying the Poisson's ratio along the material. Both shapes are visible for a part of the Poisson's ratio variant cosine 1D. This indicates that by properly selecting the parameters of the Poisson's ratio distribution, various shapes can be achieved. Furthermore, by applying a moment M_x , more complex shapes can be achieved that require a curvature variation in both directions. An example could be the outline of a torus. However, the current analytical model is limited to a plane a small out-of-plane deformation.

For future work, it would be interesting to look into allowing for a larger displacement in the z -direction. Additionally, by introducing a displacement in x - and y -direction,

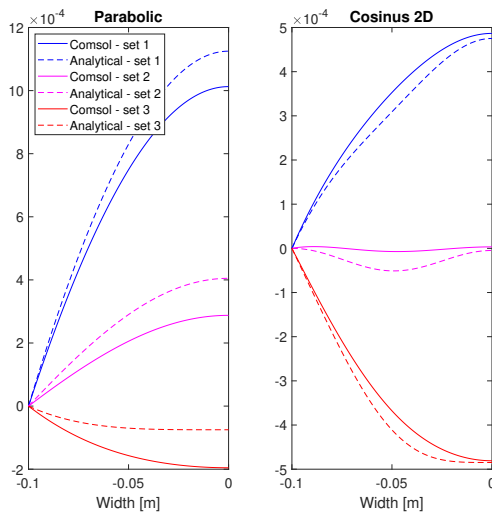


Figure 3.16: Deflection lines from the analytical and COMSOL model along the x -centerline for the parabolic and cosine 2D Poisson's ratio variants.

closed 3D shapes such as an enclosed Easter-egg or a flower vase can be achieved. These additions do require inclusion of non-linearity in the analytical model. However, firstly more Poisson's ratio variants should be implemented to strengthen the reliability of the model. To further enhance the capabilities of the model, it should be made single-symmetric or zero-symmetric.

6. Conclusion

With the growth in research on auxetic metamaterials, a realm of possibilities opened up to achieve curved shapes under out-of-plane deformation. Additionally, metamaterials allow for the Poisson's ratio to vary across the material by applying a gradient in the cellular structure. The resulting shape under out-of-plane deformation depends on the Poisson's ratio of the material. Hence, in this paper the relation between the applied load and a varying Poisson's ratio distribution is explored.

To understand the mechanical relation, an analytical model is setup for a pure bending load case on a square plate. The plate is minimally constrained to allow deformation based on material properties. The same model is incorporated in the FEM software COMSOL for comparison and is noted as the reference model.

Within the analytical model and the COMSOL model, four Poisson's ratio distributions were applied, with three Poisson's ratio range-sets per distribution.

The analytical model showed promising results with the Mean Absolute Percentage Error (MAPE) in an acceptable range. The MAPE accuracy ranges from 0.30% to 11.93%. Interestingly, the Poisson's ratio distributions that vary in one direction show a higher accuracy with the Mean Absolute Percentage Error (MAPE) being below one percent point. When the Poisson's ratio distribution also varies in the second direction, the accuracy decreases. The decrease is probably caused by the increase in Poisson's ratio variation. Important to note is that the largest values for the Mean Absolute Error (MAE)'s are concentrated

along the edges. The location is attributed to peak in curvature occurring in the COMSOL result, possibly due to an error in the FEM computation.

Furthermore, applying a variation in the Poisson's ratio has shown that the material can deform to a double-curved or dome-like shape. To achieve a desired shape, the distribution of the Poisson's ratio can be adjusted. The analyzed analytical model had an applied moment along one direction, limiting the effect of the Poisson's ratio along one direction. Applying a second moment along the perpendicular direction would provide more shape variations.

Future work would focus on refining the analytical model by applying more Poisson's ratio variants and by adding a moment along the x -direction. To further extend the capabilities of the model, a displacement along the x - and y -direction and a larger displacement in the z -direction can be incorporated. Moreover, this may offer more complex deformation shapes but will require introducing non-linearity into the model.

In conclusion, valuable insights are presented into the potential of a varying Poisson's ratio distribution on the out-of-plane deformation behavior. This study shows a first step into the direction of bending a flat plane into a sphere using auxetic metamaterials.

Bibliography

- [1] A. A. Zadpoor, "Mechanical -performance of additively manufactured meta-biomaterials," *Acta biomaterialia*, vol. 85, pp. 41–59, 2019.
- [2] A. A. Zadpoor, "Mechanical meta-materials," *Materials Horizons*, vol. 3, no. 5, pp. 371–381, 2016.
- [3] I. Masters and K. Evans, "Models for the elastic deformation of honeycombs," *Composite structures*, vol. 35, no. 4, pp. 403–422, 1996.
- [4] N. Novak, M. Vesenjajk, and Z. Ren, "Auxetic cellular materials-a review," *Strojniški vestnik-Journal of Mechanical Engineering*, vol. 62, no. 9, pp. 485–493, 2016.
- [5] R. Lakes, "Foam structures with a negative poisson's ratio," *Science*, vol. 235, no. 4792, pp. 1038–1040, 1987.
- [6] M. Sanami, N. Ravirala, K. Alderson, and A. Alderson, "Auxetic materials for sports applications," *Procedia Engineering*, vol. 72, pp. 453–458, 2014.
- [7] S. J. Callens and A. A. Zadpoor, "From flat sheets to curved geometries: Origami and kirigami approaches," *Materials Today*, vol. 21, no. 3, pp. 241–264, 2018.
- [8] L. H. Dudte, E. Vouga, T. Tachi, and L. Mahadevan, "Programming curvature using origami tessellations," *Nature materials*, vol. 15, no. 5, pp. 583–588, 2016.
- [9] M. J. Mirzaali, A. Ghorbani, K. Nakatani, M. Nouri-Goushki, N. Tümer, S. J. Callens, S. Janbaz, A. Accardo, J. Bico, M. Habibi, *et al.*, "Curvature induced

- by deflection in thick meta-plates,” *Advanced materials*, vol. 33, no. 30, p. 2008082, 2021.
- [10] R. La Magna and J. Knippers, “Tailoring the bending behaviour of material patterns for the induction of double curvature,” in *Humanizing Digital Reality: Design Modelling Symposium Paris 2017*, pp. 441–452, Springer, 2018.
- [11] R. Naboni, S. Sartori, and L. Mirante, “Adaptive-curvature structures with auxetic materials,” in *Advanced Materials Research*, vol. 1149, pp. 53–63, Trans Tech Publ, 2018.
- [12] Y. Sakai and M. Ohsaki, “Optimization method for shape design of auxetic bending-active gridshells using discrete differential geometry,” in *Structures*, vol. 34, pp. 1589–1602, Elsevier, 2021.
- [13] S. P. Timoshenko and S. Woinowsky-Krieger, *Theory of plates and shells*. McGraw-Hill International editions, 2 ed., 1959.
- [14] J. Stewart, *Calculus early transcendentals - international edition*. Cengage Learning, 7 ed., 2012.
- [15] “Azo materials.” Retrieved on 03-02-2023 from <https://www.azom.com/properties.aspx?ArticleID=920>.
- [16] “Freepik.” Retrieved on 26-06-2023 from https://www.freepik.com/free-vector/hand-drawn-easter-day-eggs-with-happy-colours_6839366.htm#query=easter%20egg&position=0&from_view=keyword&track=ais.
- [17] “Freepik.” Retrieved on 26-06-2023 from https://www.freepik.com/free-vector/lovely-flowers-collection-with-flat-design_3242929.htm#page=4&query=flower%20vase&position=23&from_view=search&track=ais%22%3EFreepik%3C/a.
- [18] F. van Keulen, *Advanced Mechanics Part: Continuum Mechanics and Nonlinear Mechanics (first part)*. TU Delft, 1 ed., 2017.

A

Poisson's ratio gradient and the corresponding displacement field

A.1. S-curve

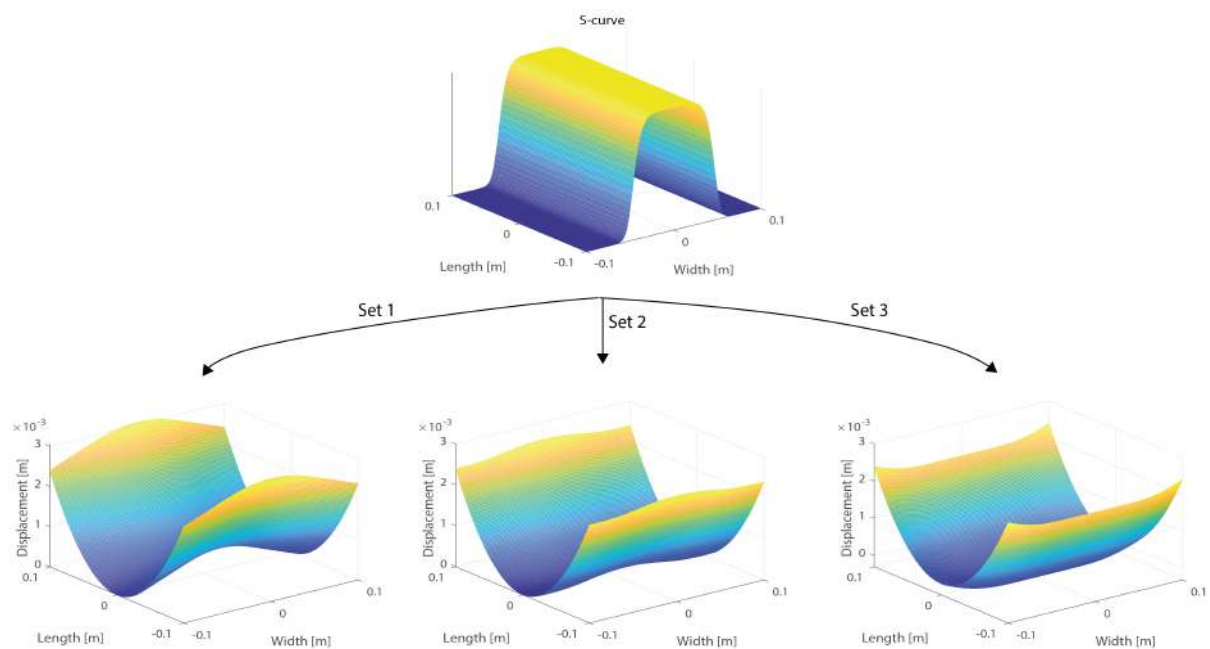


Figure A.1: The three displacement fields resulting from pure bending of a plate containing S-curve Poisson's ratio variation.

A.2. Parabolic

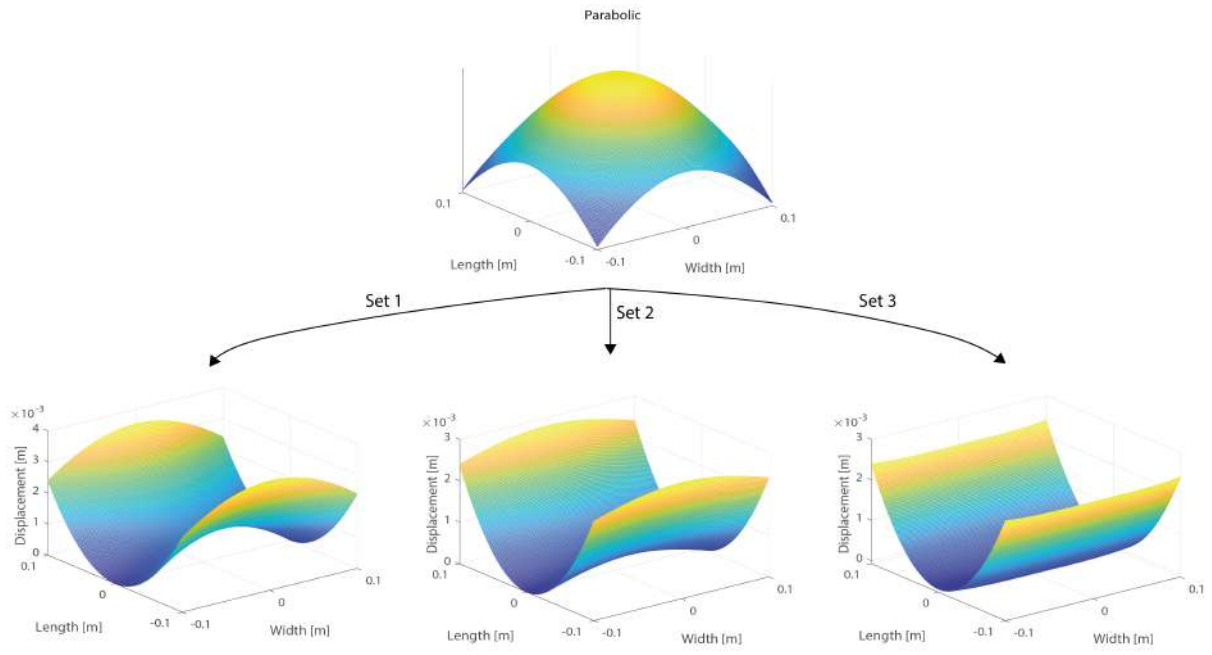


Figure A.2: The three displacement fields resulting from pure bending of a plate containing Parabolic Poisson's ratio variation.

A.3. Cosine 1D

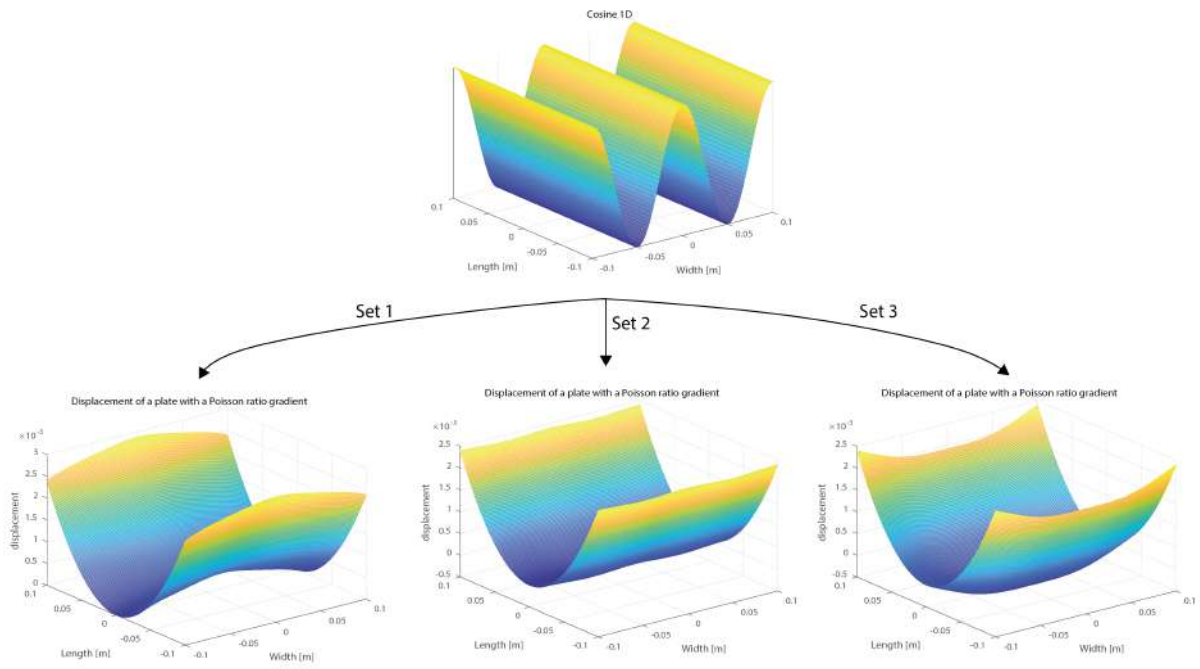


Figure A.3: The three displacement fields resulting from pure bending of a plate containing cosine 1D Poisson's ratio variation.

A.4. Cosine 2D

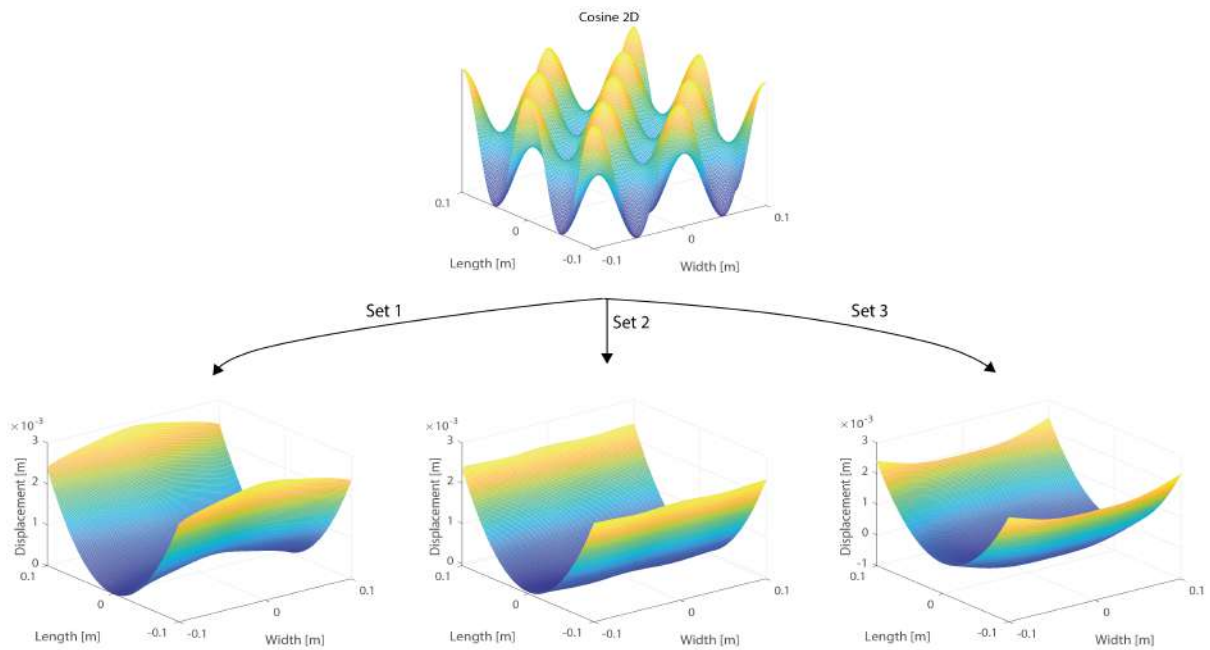


Figure A.4: The three displacement fields resulting from pure bending of a plate containing cosine 2D Poisson's ratio variation.

B

Comsol data-processing

```
function Z = comsoldata(d)

n = 201;
x = d(:,1);
z = d(:,3);
y = d(:,2);
xv = linspace(min(x), max(x), n);
yv = linspace(min(y), max(y), n);
[X,Y] = meshgrid(xv, yv);
Z = griddata(x,y,z,X,Y, 'v4');
end
```

C

Matlab code

```
%% Pure bending with Poisson ratio gradient

%Set the parameters
parameters_poissongradient;

%Set the matrices for ddx, ddy, dx, dy and w
ddx_e = NaN(length(x),length(y));
ddy_e = NaN(length(x),length(y));
D_e = NaN(length(x),length(y));

%Comptue the values for D, ddx and ddy
for i = 1:length(x)
    for j = 1:length(y)
        D_e(i,j) = (E*h^3)/(12*(1-v(i,j)^2));
        ddx_e(i,j) = -(Mx-v(i,j)*My)/(D_e(i,j)*(1-v(i,j)^2));
        ddy_e(i,j) = -(My-v(i,j)*Mx)/(D_e(i,j)*(1-v(i,j)^2));
    end
end

%Determine the values for dx and dy through numerical integration
[w_e,dx_e,dy_e] = euler_numerical(ddx_e,ddy_e,f);

%% General parameters
E = 25*10^6; % [Pa], Youngs modulus material
    Silicone
b = 0.2; % [m], width of the plate
h = 10*10^-3; % [m], heigth of the plate
% F = -5; % [N], applied load
L = 0.2; % [m], length of the plate
s = 10^-3; % step size
x_1 = 0:s:L/2; % x-centerline till middle
y_1 = x_1; % y-centerline till middle
x = 0:s:L; % x-centerline
y = x; % y-centerline
v = poissonratio(x,y); %Poisson ratio gradient
Mx = 0; % [Nm/m], moment applied on the x-
    axis
My = -1; % [Nm/m], moment applied on the y-
    axis
f = length(y)/2+0.5; %middle point

function v = poissonratio(x,y)
x = -0.1:10^-03:0.1;
```

```

y = x;
a = length(x);
b = length(y);

%Uncomment the desired Poisson's ratio variant

%S-curve
% k = 200;
% t = 2;
% v = NaN(a,a);
% for i=1:a
%     if x(i)<0
%         v(:,i)=2/5*1/(1+exp(-k*(x(i)+0.05)))^t-0.4;
%     else
%         v(:,i)=2/5*1/(1+exp(k*(x(i)-0.05)))^t-0.4;
%     end
% end

%Parabolic
% A=0.1;
% B=0.1;
% constant = 1; % or 0, whichever you want.
% v2 = -0.4;
% C=sqrt((v2)^2/constant);
% numElements = a;
% % Define range of x and y axes.
% x = linspace(-A, A, numElements);
% y = linspace(-B, B, numElements);
% % Get every possible combination of x and y.
% [X, Y] = meshgrid(x, y);
% % Construct function.
% v = -C * sqrt(constant + X.^2 / A^2 + Y.^2 / B^2)+0.4;
% v = reshape(v, [], b);
%
% minimum = min(v,[],'all');
% maximum = max(v,[],'all');
% M = abs(minimum-maximum);

%Cos 1D
% numElements = a;
% A=0.1;
% B=0.1;
% % Define range of x and y axes.
% x = linspace(-A, A, numElements);
% y = linspace(-B, B, numElements);
% % Get every possible combination of x and y.
% [X, Y] = meshgrid(x, y);
% v = 2/10*cos((2*pi/0.1).*X);

%Cos 2D
%numElements = a;
% A=0.1;
% B=0.1;
% %Define range of x and y axes.
% x = linspace(-A, A, numElements);
% y = linspace(-B, B, numElements);
% %Get every possible combination of x and y.
% [X, Y] = meshgrid(x, y);
% v = 2/10*cos((2*pi/0.1).*X).*cos((2*pi/0.1).*Y)-0.2;

end

```

```

function [w,dx,dy] = euler_numerical(ddx,ddy,f)

%Retrieve the required parameters
parameters_poissongradient;

%Set the matrix for dx, dy, w
dx = NaN(length(x),length(y));
dy = NaN(length(x),length(y));
w = NaN(length(x),length(y));

%Set the node attached to the rotation joint to zero
w(length(x)/2+0.5,1) = 0;

%Set the nodes of the slope along the double-symmetry line to zero
dx(:,f) = 0;

%Determine the slope dw/dx of the quarter field
for j = f:2*f-1
    for i = 1:f-1
        dx(j,f-i) = dx(j,f-i+1)-s*ddx(j,f-i);
    end
end

%Determine the deflection along the x-centerline
for j = 2:f
    w(f,j) = w(f,j-1)+dx(f,j-1)*s+ddx(f,j-1)*s^2/2;
end

%Set the nodes of the slope along the double-symmetry line to zero
dy(f,:) = 0;

%Determine the slope dw/dy of the quarter field
for j = 1:f
    for i = 1:f-1
        dy(f+i,j) = dy(f+i-1,j)+s*ddy(f+i-1,j);
    end
end

%Determine the remaining deflection of the quarter field
for i = f+1:2*f
    for j = 1:f
        w(i,j) = w(i-1,j)+dy(i-1,f)*s+ddy(i-1,f)*s^2/2;
    end
end

%Construct the whole field by mirroring the quarter two times
w(1:f,:) = flip(w(f:end,:));
w(:,f:end) = flip(w(:,1:f),2);

end

```

D

Comsol and Matlab overlap uniform Poisson's ratio

Before the Poisson's ratio variants are incorporated, the analytical model is validated in order to review if the set-up is correct. The analytical model is validated against the referenc model in the FEM software COMSOL. To determine whether the analytical set-up is accurate, the Mean Absolute Percentage Error (MAPE) is evaluated. The MAPE measures the accuracy of the analytical model as a percentage and is computed in the following way:

$$\begin{aligned} e(i, j) &= |Z(i, j) - w(i, j)| \\ p(i, j) &= \frac{e(i, j)}{|Z(i, j)|} \cdot 100 \\ \text{MAPE} &= \frac{\sum p(i, j)}{N} \end{aligned} \quad (\text{D.1})$$

The parameter $Z(i, j)$ is the deflection of the Comsol model, $w(i, j)$ is the deflection of the analytical model and N is the number of data points.

The resulting MAPE values can be seen in Figure D.1. The MAPE is evaluated for a Poisson's ratio range of $\nu = [-0.8 \ -0.6 \ -0.4 \ -0.2 \ 0 \ 0.2 \ 0.4 \ 0.6 \ 0.8]$.

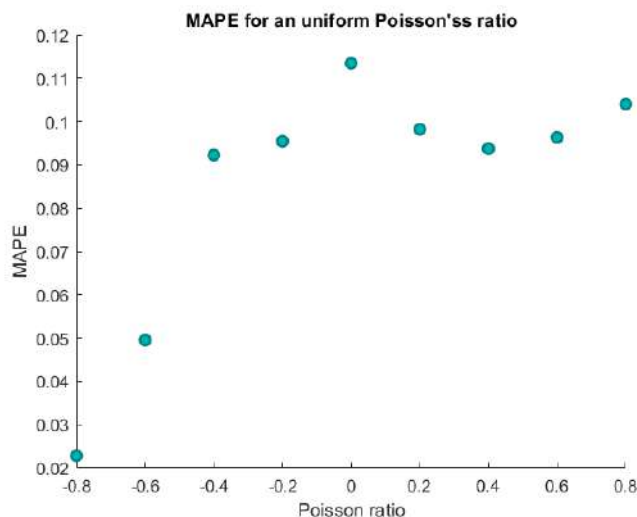


Figure D.1: The MAPE of the analytical model against the COMSOL with an uniform Poisson's ratio varying from $\nu = -0.8$ to $\nu = 0.8$.

The MAPE value for every Poisson's ratio value is below a percent point, hence the analytical set-up is considered to be validated.